NOVA SCHOOL OF SCIENCE & TECHNOLOGY

DEPARTMENT OF PHYSICS

ALEXANDRA FERREIRA CORDAS

BSc in Biomedical Engineering

DEVELOPMENT OF MESOPOROUS BIOGLASS-BASED SYSTEMS FOR CONTROLLED DELIVERY OF CYTOTOXIC DRUGS

MASTER IN BIOMEDICAL ENGINEERING

NOVA University Lisbon

September, 2024

NOVA SCHOOL OF SCIENCE & TECHNOLOGY

DEPARTMENT OF PHYSICS

DEVELOPMENT OF MESOPOROUS BIOGLASS-BASED SYSTEMS FOR CONTROLLED DELIVERY OF CYTOTOXIC DRUGS

ALEXANDRA FERREIRA CORDAS

BSc in Biomedical Engineering

Adviser: Paula Isabel Pereira Soares
Principal Researcher, NOVA University Lisbon

Co-adviser: João Paulo Miranda Ribeiro Borges
Full Professor, NOVA University Lisbon

Examination Committee:

Chair: Ricardo Nuno Pereira Verga e Afonso Vigário,
Associate Professor, NOVA University Lisbon

Rapporteur: Célia Maria Reis Henriques,
Associate Professor, NOVA University Lisbon

Adviser: Paula Isabel Pereira Soares,
Principal Researcher, NOVA University Lisbon

MASTER IN BIOMEDICAL ENGINEERING

NOVA University Lisbon
September, 2024

Development of mesoporous bioglass-based systems for controlled delivery of cytotoxic drugs

ACKNOWLEDGMENTS

Primeiramente, gostaria de agradecer à minha orientadora Doutora Paula Soares, por toda a disponibilidade fornecida ao longo da dissertação, ajuda, confiança e amabilidade. Ao professor Doutor João Paulo Borges, meu co-orientador, pelos conhecimentos transmitidos e pela paciência, aquando das inúmeras dúvidas que iam surgindo durante os procedimentos.

Um agradecimento especial à Francisca, minha companheira de bancada e de tese, por toda a companhia e ajuda dada ao longo destes meses, e que me enturmou num departamento que pouco conhecia.

Aos colegas de laboratório Adriana, Cezar, Miguel, Bernardo, Tomás, Guilherme e Marco, a todos os alunos de projeto e à Dona Augusta, que tornaram aquilo que seria um ambiente de trabalho, num espaço acolhedor, cheio de caras familiares, que não hesitavam em ajudar caso algo fosse preciso.

Às cavaleiras do apocalipse Jéssica, Márcia e Sara, que desde o primeiro ano da faculdade estiveram presentes na tempestade e na bonança, que me ergueram (até literalmente) quando mais precisei, e que serão para sempre os pilares do meu ser. Um muito obrigada por tudo.

À Carol, minha cinéfila favorita, muito obrigada por seres a minha melhor amiga. É contigo que partilho os factos mais estranhos deste mundo e as aventuras por Portugal.

Aos rapazes Adamastor, Gonçalo e Lourenço, um grande *shout-out*, pela jogatina, gargalhadas e companhia até o sol raiar.

Ao Krystian, um muito obrigada por me aceitares como sou, pela companhia, carinho e confiança.

Por último, mas não menos importante, à minha família. Aos meus avós por todo o carinho e preocupação, e à minha mãe, que tudo fez, faz e fará por mim. Que o sol da minha vida nunca passe a uma lua.

"I have no special talents. I am only passionately curious." (Albert Einstein).

ABSTRACT

Cancer remains a leading global cause of death, with over 10 million deaths annually. Osteosarcoma, a primary bone cancer, predominantly affects children and young adults, and it typically requires conventional therapies, such as radiotherapy, chemotherapy, and surgery. However, these treatments cause significant side effects and carry the risk of cancer recurrence.

This study presents the synthesis and analysis of mesoporous bioactive glasses (MBGs) doped with varying copper concentrations - 0 % (BG0), 2 % (BG2), and 5 % (BG5) mol.%, using the sol-gel method, assisted by the Evaporation-Induced Self-Assembly (EISA) technique. 25 mg of MBGs were loaded with 0.1, 0.2, and 0.4 mg/mL of doxorubicin (DOX) for controlled drug delivery studies. Characterization of the MBGs revealed median particle sizes below 3 μm, with specific surface areas ranging from 187 to 367 m^2/g, pore volumes between 0.227 and 0.393 cm^3/g, and pore diameters between 3.97 and 4.81 nm. Bioactivity studies demonstrated the formation of a hydroxycarbonate apatite layer within 7 days, highlighting its potential to promote bone regeneration. DOX encapsulation efficiencies ranged from 75.6 % for BG0 with 0.1 mg/mL of DOX to 97.1 % for BG2 with 0.4 mg/mL of DOX. The highest cumulative drug release was 18.3 % after 7 days, being inversely proportional to the copper concentration within the samples. The addition of copper enhanced anti-bacterial properties against *S. aureus* and *E. coli* bacteria, though it also increased the cytotoxicity of the samples.

This study demonstrates the potential of multifunctional MBGs for bone regeneration, controlled drug delivery, and anti-bacterial activity, providing promising results as a complementary therapy for the treatment of bone cancer.

Keywords: Bone regeneration, copper, doxorubicin, drug delivery, mesoporous bioactive glass.

RESUMO

O cancro continua a ser uma das principais causas de morte a nível global, com mais de 10 milhões de óbitos anuais. O osteossarcoma, um tipo de cancro ósseo primário, afeta predominantemente crianças e jovens adultos e, normalmente, requer terapias convencionais, como radioterapia, quimioterapia e cirurgia. No entanto, estes tratamentos causam efeitos secundários significativos e apresentam o risco de recorrência do cancro.

Este estudo apresenta a síntese e análise de vidros bioativos mesoporosos (MBGs) dopados com diferentes concentrações de cobre - 0 % (BG0), 2 % (BG2) e 5 % (BG5) mol.%, utilizando o método sol-gel, assistido pela técnica de *Evaporation-Induced Self-Assembly* (EISA). 25 mg de MBGs foram carregados com 0,1, 0,2 e 0,4 mg/mL de doxorrubicina (DOX) para estudos de libertação controlada de fármacos. A caracterização dos MBGs revelou tamanhos médios de partícula abaixo de 3 µm, com áreas de superfície específicas variando entre 187 e 367 m^2/g, volumes de poros entre 0,227 e 0,393 cm^3/g e diâmetros de poros entre 3,97 e 4,81 nm. Estudos de bioatividade demonstraram a formação de uma camada de apatite hidroxi-carbonatada em 7 dias, evidenciando o seu potencial para promover a regeneração óssea. As eficiências de encapsulamento de DOX variaram de 75,6 % para o BG0 com 0,1 mg/mL de DOX até 97,1 % para o BG2 com 0,4 mg/mL de DOX. A maior libertação cumulativa de fármaco foi de 18,3 % após 7 dias, sendo inversamente proporcional à concentração de cobre nas amostras. A adição de cobre melhorou as propriedades antibacterianas contra as bactérias *S. aureus* e *E. coli*, embora também tenha aumentado a citotoxicidade das amostras. Este estudo demonstra o potencial dos MBGs multifuncionais para a regeneração óssea, libertação controlada de fármacos e atividade antibacteriana, apresentando resultados promissores como terapia complementar para o tratamento do cancro ósseo.

Palavras-chave: Cobre, doxorrubicina, libertação de fármaco, regeneração óssea, vidro bioativo mesoporoso.

CONTENTS

LIST OF FIGURES

List of Tables

List of Abbreviations

ATR	Attenuated Total Reflectance
BET	Brunauer–Emmett–Teller
BG	Bioactive Glass
CFU	Colony-Forming Unit
CMA	Concomitant Metals Analyzer
DMSO	Dimethyl Sulfoxide
DOX	Doxorubicin
DOX@MBG	Mesoporous Bioactive Glass with Doxorubicin
EDS	Energy Dispersive Spectroscopy
EE	Encapsulation Efficiency
EISA	Evaporation Induced Self-Assembly
FTIR	Fourier Transform Infrared Spectroscopy
HA	Hydroxyapatite
HCA	Hydroxycarbonate Apatite
ICP	Inductively Coupled Plasma
LDA	Laser Diffraction Analysis
MBG	Mesoporous Bioactive Glass
PBS	Phosphate Buffered Saline
P-123	Pluronic 123
SaOs	Sarcoma Osteogenic
SBF	Simulated Body Fluid
SEM	Scanning Electron Microscopy
STEM	Scanning Transmission Electron Microscopy

TEOS	Tetraethyl Orthosilicate
TEP	Triethyl Phosphate
TSB	Tryptic Soy Broth
UV-VIS	Ultraviolet Visible
XRD	X-Ray Diffraction

1

INTRODUCTION

1.1 Scientific context

Cancer is a disease where abnormal cells grow uncontrollably, forming a mass of tissue called a tumor. The malignant tumor can invade nearby tissues and spread to other body parts through the bloodstream or lymphatic system, leading to metastasis [1].

In 2022, there were 20 million new cases of cancer, and almost half of them led to death, suggesting that one in five individuals will eventually develop cancer in a lifetime, and one in ten will die [2].

Among the various types of cancer, osteosarcoma is a primary bone cancer that typically affects children and young adults [3]. Although primary bone cancer is relatively uncommon, accounting for just 1% of all cancer cases, this type of cancer is extremely difficult to eliminate, requiring conventional therapies such as radiotherapy, chemotherapy, and surgery [4]. However, these treatments come with numerous short- and long-term side effects, having some risk of recurrence of cancer cells [5].

Therefore, there is a need to discover new therapeutic approaches that are less invasive and provide well-being to the patient both during and after treatment.

1.2 Bioactive glass

Conventional bioactive glass (BG), or bioglass, is an amorphous ceramic biomaterial characterized by its bioactivity, as it is compatible with the human body [6]. When in contact with body fluid, it induces the formation of hydroxyapatite (HA) on its surface, which is the primary

mineral component of bone [7]. Thus, it is commonly used for bone regeneration, as it has the property of bonding with bone and stimulating bone growth [6].

Bioglass is typically synthesized using two methods: the melt-quenching method and the sol-gel method. However, the sol-gel method has been observed to have more advantages, as it requires a lower temperature for synthesis, is easier to synthesize, and results in higher homogeneity and purity of the final products. It also allows for adjustable porosity and a wider range of compositional variations. The melt-quenching method, by contrast, limits silica content to a maximum of 60 mol.%, whereas the sol-gel method can achieve bioglasses with up to 90 mol.% silica [8].

However, even with these advantages, bioglass has some limitations. It lacks uniformity in pore structure and does not have certain clinical capabilities, such as controlled drug release. To overcome these limitations, mesoporous bioglass (MBG) was produced using the sol-gel method, which features porosity between 2 and 50 nm. This type of bioglass is characterized by a large pore volume (1 cm^3/g) and a large surface area (greater than 100 m^2/g) with a well-defined surface. These properties enhance interactions between the bioglass, biological fluids, and cells, facilitating the adsorption of proteins and accelerating the formation of the apatite layer [9].

The increased surface area and pore volume of mesoporous bioglass results in a highly ordered arrangement of uniformly sized pores, enabling controlled drug release [10].

To produce MBG using the sol-gel method, Evaporation Induced Self-Assembly (EISA) is employed, with the non-ionic surfactant Pluronic playing a key role. During the stirring of the solution at room temperature, solvent evaporation occurs, causing the solution to gradually transition into a gel. In this process, Pluronic molecules self-organize into micelles that interact with the hydrolyzed silica precursors through their hydrophilic components, leading to the formation of an ordered mesophase [11]. Pluronic P-123, an amphiphilic surfactant, facilitates the self-assembly process and aids in the adsorption of lipophilic drugs onto the bioactive glass. This surfactant is advantageous due to its low toxicity and a molecular size that reduces the risk of renal excretion [9].

To impart multifunctionality onto the mesoporous bioglass, it is possible to add metal ions, such as copper, silver, zinc, and others. Copper is naturally present in human tissues and is essential for various biological processes. This was the chosen ion to take part in the synthesis since it is the only ion that possesses all three desired biological properties to include in the system: osteogenic (promoting bone tissue growth and regeneration), angiogenic (promoting

the formation of new blood vessels), and anti-bacterial (inhibiting the growth and survival of bacteria, thus helping prevent infections) [12], [13].

1.3 Drug delivery systems

A drug delivery system refers to a formulation or device designed to introduce a drug into the body for administration and absorption. The aim of drug delivery systems is to provide a therapeutic dose of medication while enhancing safety and effectiveness by controlling the specific location, rate, and timing of the drug's release within the body [14].

To ensure the system can effectively target any remaining tumor cells that were not removed by conventional treatments, it is essential for a cytotoxic drug to be adsorbed onto the surface of the bioglass.

Doxorubicin (DOX), an antibiotic derived from the bacterium *Streptomyces peucetius*, has been used as a chemotherapeutic agent since the 1960s, being commonly used to treat soft tissue and bone sarcomas, as well as cancers of the breast, ovary, bladder, and thyroid. Doxorubicin primarily functions by intercalating between DNA base pairs, which breaks DNA strands and prevents the synthesis of both DNA and RNA. Additionally, it inhibits the activity of topoisomerase II, which damages DNA and triggers apoptosis [15].

1.4 State of the art

Conventional bioglass, first manufactured by Hench *et al.* in 1971, was named 45S5 Bioglass ®, with a composition of 46.1 % SiO_2 (silicon dioxide), 24.4 % Na_2O (sodium oxide), 26.9 % CaO (calcium oxide), and 2.6 % P_2O_5 (phosphorus pentoxide) in mol.%. When tested *in vivo*, it was observed that the bond between the cortical bone and the glass was equal to, or even stronger than the bone itself, making the removal of the bioglass quite difficult [6].

Through new studies, other compositions were tested, concluding that increasing the specific surface area and pore volume led to greater bioactivity of the bioglass, as it accelerated the deposition of the apatite layer on the surface of the bioglass, enhancing the ability to stimulate new bone growth [16].

Mesoporous bioglass was first synthesized in 2004 by Yan *et al.* [16]using the sol-gel method and non-ionic copolymers to achieve an ordered structure through the EISA process, where the solvent evaporates, directing the bioglass structure. It was demonstrated that

mesoporous bioglasses allowed for greater bioactivity than traditional bioglass, leading to more bone formation and possessing more homogeneity [16].

According to the review article by Migneco *et al.* [9], a collection of different concentrations of the Ca/P/Si (Calcium/Phosphorus/Silicon) ratio, with and without incorporated ions, was analyzed. It was concluded that Ca^{2+} ions are responsible for excellent and rapid bioactivity when in contact with simulated body fluid (SBF), and CaO is related to the efficiency of drug kinetics adsorbed on the bioglass surface. Regarding phosphorus, it was concluded that a concentration around 5 mol.% was beneficial for the mesopore structural design [9].

In addition to the major components of mesoporous bioglasses, it is pertinent to study the introduction of small amounts of metallic ions to impart multifunctionality to them. *In vitro* and *in vivo* tests demonstrate that it is possible to stimulate an angiogenic response with the addition of copper, cobalt, and boron ions, an anti-bacterial response with zinc, copper, cerium, gallium, and silver ions, an osteogenic response with zirconium, boron, iron, magnesium, lithium, strontium, cobalt, copper, cerium, and gallium ions, and finally, a cementogenic response with lithium and strontium ions [12].

However, the addition of these ions leads to a decrease in the specific surface area and pore volume of the final mesoporous bioglasses, as their incorporation negatively impacts the condensation of precursors, destabilizing the ordered orientation of silicate units. Therefore, their addition must be done carefully to avoid compromising the homogeneity and integrity of the bioglass being developed [9].

Additionally, studies have been conducted to adjust the porosity, pore size, and increase the surface area, making them not only interesting for bone regeneration but also for controlled drug release to treat tumors [17].

Wu *et al.* [18] successfully synthesized mesoporous bioglass nanospheres with a Ca/P/Si ratio of 15/5/80 using the hydrothermal method, achieving a surface area and mesopore volume of 443 m^2/g and 0.57 cm^3/g, respectively, with a uniform mesopore size distribution of 2.9 nm. These nanospheres revealed approximately 90 % efficiency in the adsorption of the cytotoxic drug doxorubicin, whereas it was previously difficult to achieve more than 50 % of drug adsorption. These were tested on Sarcoma osteogenic (SaOs) cells, significantly inhibiting them, and the drug release kinetics were effectively controlled by the initial drug concentration and the pH of the medium [18].

Another synthesis that yielded promising results was achieved Rahman *et al.* [19], where mesoporous bioglass nanoparticles were doped with silver ions, synthesized using the sol-gel method with a composition of SiO_2 (51 %), CaO (20 %), Na_2O (20 %), P_2O_5 (4 %), and Ag_2O (5

%) mol.%, showing good results in bone regeneration and doxorubicin release. The encapsulation efficiency of DOX was 84 %, with its release observed between concentrations of 0.2-1.0 mg/mL, within a pH range of 6.4-8.4. The release achieved was 93 % over approximately two weeks at a pH of 6.4 [19].

The ongoing challenge lies in optimizing the synthesis of mesoporous bioglasses while incorporating ions and enhancing their ability to adsorb cytotoxic drugs, allowing them to serve as an effective drug delivery system. This approach aims to maximize their properties, with the potential to support conventional therapies for bone cancer.

The purpose of this work is to develop multifunctional mesoporous bioactive glasses capable of adsorbing a cytotoxic drug onto their surface. The system is placed at the previous site of the bone tumor following surgery, enabling controlled drug release to prevent the recurrence of cancer cells, with subsequent bone regeneration, so that new healthy bone cells can be formed as quickly as possible. Therefore, bioglasses with 0, 2, and 5 mol.% of copper will be synthesized using the sol-gel method, assisted by EISA technique. These bioglasses will then be loaded with DOX at concentrations of 0.1, 0.2, and 0.4 mg/mL. Once the powders are obtained, the samples will undergo characterization using various analytical techniques. Bioactivity, anti-bacterial, and cytotoxicity assays, as well as encapsulation and release studies of doxorubicin, will be conducted to evaluate the potential of the bioactive glasses for bone regeneration, controlled drug delivery, and anti-bacterial properties. These studies will reveal the impact of copper incorporation into the bioglass and evaluate whether or not these MBGs can be implemented as a system for the controlled delivery of cytotoxic drugs, in order to help as a complementary therapy for the treatment of bone cancer.

The research work described in this dissertation was carried out in accordance with the norms established in the ethics code of Universidade Nova de Lisboa. The work described and the material presented in this dissertation, with the exceptions clearly indicated, constitute original work carried out by the author.

2

MATERIALS AND METHODS

2.1 Synthesis of copper-doped bioactive glass

Mesoporous bioglass was produced by sol-gel method assisted by EISA, using tetraethyl orthosilicate ($C_4H_{20}O_{10}Si$, TEOS, *Sigma-Aldrich*), triethyl phosphate ($(C_2H_5)_3PO_4$, TEP, *Fluka*), calcium nitrate tetrahydrate ($Ca(NO_3)_2.4H_2O$, *Panreac AppliChem*) and copper (II) chloride dihydrate ($CuCl_2.2H_2O$, *Merck*) as inorganic precursors, Pluronic (P-123, *Sigma-Aldrich*) as the surfactant, and ethanol (*Honeywell*, 99.8 %) as solvent.

Three different MBGs were synthesized, where the difference relies on the amount of copper and calcium used, where the molar fraction is represented by Cu/Ca/P/Si. Therefore, the ratio for bioglass without copper, BG0, was 0/15/5/80, the bioglass with 2 mol.% copper, BG2, was 2/13/5/80, and finally, with 5 mol.% copper was 5/10/5/80, BG5.

Following a similar synthesis performed by Wu *et al.* [20], for BG5, 20 g of TEOS, 2.83 g of $Ca(NO_3)_2.4H_2O$, 2.19 g of TEP, and 1.02 g of $CuCl_2.2H_2O$ were added to 120 mL of ethanol. Then 1 mL of 0.5 M HCl (hydrochloric acid) solution was added, and the mixture was left stirring until the salts were completely dissolved. Finally, 8 g of surfactant P-123 was added. The solution was left at room temperature for three days under magnetic stirring. Once the solution became a gel, it was kept at 80 °C for three days, until the ethanol had completely evaporated. Once the product was similar to glass, it was ground in a mortar and then placed in a furnace at 700 °C for 5 hours, to evaporate the surfactant. For the other two bioglasses, the protocol used was the same, simply changing the amount of Cu and Ca used, following its stoichiometric equations.

Finally, the powder of the MBGs was achieved by a zirconia ball milling technique, using a planetary ball mill, for 6 hours. The powders were ground in periods of 30 minutes at 400

rpm and using a 1:1 ratio of ethanol and grams of bioglass. Once the procedure was completed, ethanol was used to be able to separate the powder from the zirconia balls and was finally left to dry at 60 °C, getting the final powder product.

2.2 Synthesis of the drug release system

For the synthesis of the bioglasses with doxorubicin (DOX@MBGs), the protocol was adapted from Wu *et al.* [18]. First, a 7.4 pH phosphate buffer solution (PBS) was made following the protocol followed by Paula Soares [21], section 7.2.1. Then, DOX was dissolved in PBS (DOX-PBS) to make a stock solution of 0.4 mg/mL. Subsequently, 25 mg of each of the bioglasses produced (BG0, BG2, and BG5) were soaked in a 2 mL DOX-PBS solution, with concentrations of 0.4 mg/mL, 0.2 mg/mL and 0.1 mg/mL, making the necessary dilutions out of the stock solution. The solutions were left under magnetic stirring for 24 hours. Three samples of each concentration for each one of the bioglasses were made and used for both encapsulation efficiency and release studies.

2.3 DOX calibration curves

Doxorubicin calibration curves in ultrapure water and in PBS 7.4 pH were made to determine the peak of DOX concentration, by measuring its absorbance by UV-VIS (Ultraviolet Visible) spectrophotometer (UV-VIS, T90+ PG Instruments), with a range of concentrations between 2 and 50 µg/mL of DOX, detailed in section A.1 of the Appendix. The maximum absorbance peak at 480 nm, as shown in Figure 1, obtained using concentrations between 2 and 100 µg/mL, was used for further assays, and the equations provided from absorbance as a function of concentration were used throughout the work. Each measurement was made in triplicates.

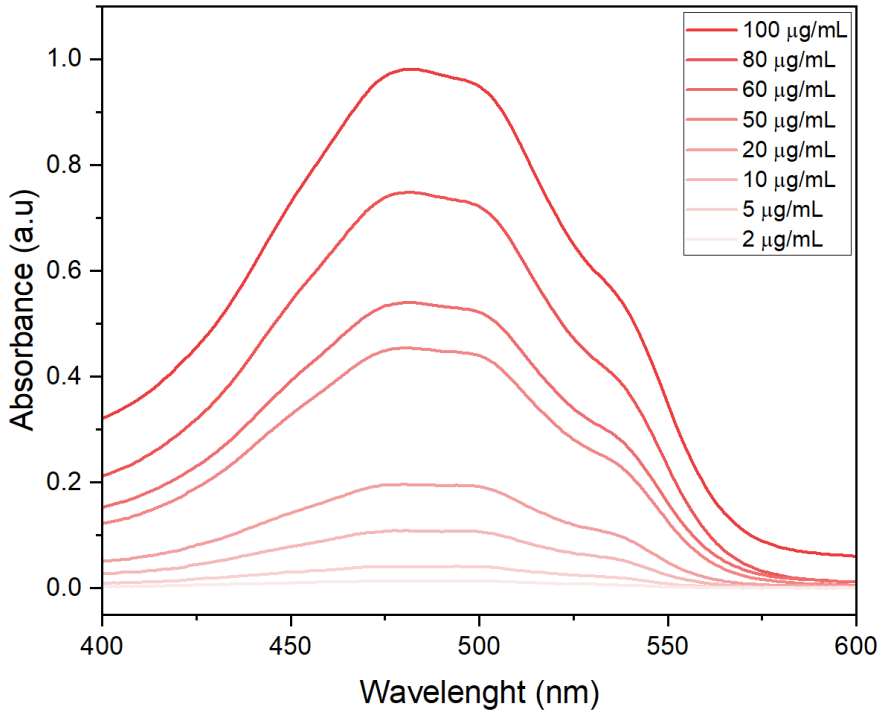

Figure 1 - Evolution of doxorubicin curves at different concentrations, from 2 µg/mL to 100 µg/mL, showing a maximum absorbance peak around 480 nm.

2.4 DOX encapsulation efficiency studies

After soaking for 24 hours, the solutions were centrifuged at 8000 rpm for 15 minutes to remove the supernatant from the samples. Then, 2 mL of ultrapure water was added to the pellets, centrifuged again, and the supernatant was removed. Both supernatants (PBS and ultrapure water) were preserved to measure their absorbance by UV-VIS spectroscopy at 480 nm. The DOX@MBG pellets were left to dry overnight at 37 °C.

2.5 DOX release studies

For DOX release test, the DOX@MBG pellets were soaked in 5 mL of fresh PBS at 37 °C, for different periods of time (3 hours, 8 hours, 24 hours, 48 hours, 72 hours, and 7 days). Then, at each timestamp, 2 mL of PBS was taken out to measure its absorbance, and 2 mL of fresh PBS was added. The cumulative release of DOX was then calculated.

2.6 Bioactivity

Simulated body fluid (SBF) with 7.4 pH was prepared following a SBF protocol [22]. Cylinder samples of 0.5 g and a superficial area of 52 cm^2 were immersed in 50 mL of SBF and kept at 37 °C in an incubator for periods of time of 3 hours, 8 hours, 24 hours, 48 hours, 72 hours, and 7 days. After each timestamp, 1 mL was analyzed by Inductively Coupled Plasma (ICP), and the samples were flushed with ultrapure water to remove any remaining salt on their surface and dried at 120 °C overnight. The samples were then observed in Scanning Electron Microscopy (SEM).

2.7 Non-passivated and passivated extracts

For both bacterial and cytotoxic assays, each MBG was used to make extracts, starting with a concentration of 100 mg/mL.

The non-passivated extracts (BG0, BG2, BG5) were obtained by sterilizing the samples (120 °C for 2 h), adding either McCoy 5A medium, for cytotoxic assays, or Tryptic Soy Broth (TSB), for bacterial assays, centrifugating them (5 minutes with 6000 rpm), filtering them with a syringe with a 0.22 µm Millipore filter attached, and then incubating them (24 hours at 37 °C). The pellets achieved in the centrifugation were preserved and added to the initial samples to be used for the passivated extracts (BG0_P, BG2_P, BG5_P), therefore having a total of 48 hours of incubation, and then a filtration.

2.8 Anti-bacterial assays

The anti-bacterial assays of the MBGs were performed in Gram-positive *Methicillin-resistant Staphylococcus aureus* and Gram-negative *Escherichia coli* bacteria, following the standard ISO 20776-1 guidelines. Each bacteria test used 2 replicates for each tested concentration, making a total of 48 well-plates per bacteria, and was repeated 3 times under the same conditions to ensure the reliability and reproducibility of the results.

The microorganisms were diluted to a concentration of 5×10^5 CFU/mL by mixing 2.4 µL of the bacterial suspension with 12 mL of TSB. For each well plate, 150 µL of this bacterial solution was combined with 300 µL of extract and 2 µL of a microorganism suspension made of 15 µL of bacteria and 485 µL of TSB. After homogenizing the mixture, serial dilutions were performed to achieve final concentrations of 100, 50, 25, and 12.5 mg/mL, by transferring 150

µL from one column to the next, discarding the final 150 µL after the last column. For the controls, 3 wells were prepared by adding 150 µL of TSB, and 3 wells were prepared by adding 150 µL of the bacterial solution. The plates were then incubated at 37 °C for 18 hours. 10 µL of the wells with no bacterial growth were subsequently transferred to a petri dish with agar and incubated overnight. Colony-Forming Units (CFUs) were then observed to assess any bacterial growth.

2.9 Cytotoxicity assays

To evaluate the cytotoxicity of the MBGs, the assays were performed according to the standard ISO-10993-5. The assays were performed using resazurin on Sarcoma Osteogenic - 2 (SaOs-2) cell line, derived from osteosarcoma cells of primary bone cancer, and performing UV-VIS spectroscopy at wavelengths of 570 nm (resorufin absorbance peak) and 600 nm (resazurin absorbance peak).

All the extracts were incubated for 48 hours at 37 °C with a 5 % CO_2 (carbon dioxide) atmosphere, using a density of SaOs-2 cells of 30 kcel/cm^2. Each extract started with a concentration of 100 mg/mL, in which three factor 2 dilutions were made, having each concentration 4 replicas (96 well plates in total).

After the incubation of the extracts, each well was aspirated, and a solution containing resazurin, composed of culture medium and a resazurin solution at a concentration of 0.04 mg/mL in a 1:1 ratio, was added. The positive control was made by using SaOs-2 in a cytotoxic environment, by adding 10 % dimethyl sulfoxide (DMSO), and the negative control by using the solution of healthy SaOs-2 cells. The medium control was prepared using the same solution as the extracts. All controls had 4 replicas, with a volume of 100 µL per well.

After 3 hours of incubation, the cell viability results were visible, where each well presented a color: pink if the cells were alive (indicating that resazurin was reduced to resorufin) or blue if the cells were dead. The absorbances of each well were measured in a Biotek ELX800 microplate reader.

2.10 Samples characterization

Fourier Transform Infrared Spectroscopy (FTIR) measurements were conducted using an Attenuated Total Reflectance (ATR) accessory fitted with a single bounce diamond crystal

on a Thermo Nicolet SummitX Spectrometer. The spectra were recorded with an incident angle of 45° across the range of 4000 to 400 cm^{-1}, with a resolution of 4 cm^{-1}.

The samples' structural characterization was carried out using X-Ray Diffraction (XRD) on a PANalytical MPD X'Pert PRO powder diffractometer equipped with a Cu Kα radiation source (λ = 1.540598 Å) and a 1D X'Celerator detector. The XRD data were collected over a 2θ range of 10 to 65° in the Bragg–Brentano geometry, with a scanning step size of 0.033°.

For Brunauer-Emmett-Teller (BET) analysis, the samples were pre-degassed at 200 °C for a minimum of 6 hours and analyzed with nitrogen as the adsorption gas at 77 K. The analyses were performed using a Micromeritics ASAP 2010 instrument.

Scanning Transmission Electron Microscopy (STEM) imaging was conducted using a Hitachi HF5000 field-emission scanning transmission electron microscope (Mito, Japan) operated at 200 kV. A drop of the sonicated dispersions was placed onto 200-mesh lacey-carbon copper grids and left to dry prior to analysis.

Laser Diffraction Analysis (LDA) was performed using a Mastersizer Hydro 2000MU (Malvern Instruments), which is designed for characterizing particle suspensions ranging from 20 nm to 2.000 µm, using a wet dispersing unit. This instrument employs laser diffraction (laser granulometry) to determine particle size.

Scanning Electron Microscopy (SEM) was performed using a Hitachi TM3030 Plus, and elemental analysis was conducted using Energy Dispersive Spectroscopy (EDS) with a Bruker XFlash MIN SVE.

Inductively Coupled Plasma (ICP) was performed using a Horiba Jobin-Yvon, France, Ultima, model equipped with a 40.68 MHz RF generator, Czerny-Turner monochromator with 1.00 m (sequential), autosampler AS500 and Concomitant Metals Analyzer (CMA) for the determination of calcium (Ca), phosphorus (P), silicon (Si), and copper (Cu), in the ppb range, simultaneously with other elements. The samples were analyzed in 1 mL of aqueous solution (SBF).

3

RESULTS AND DISCUSSION

3.1 Production of MBG

In this work, MBGs were synthesized using the sol-gel method assisted by EISA, with Pluronic P-123 as the surfactant. Figure 2 presents the different stages of MBG production, arranged according to the copper content: BG0 on the left, BG2 in the center, and BG5 on the right. The first stage, shown in Figure 2 a), represents the sol-gel form of the MBGs after 48 hours of synthesis. The samples were stirred magnetically for 3 days at room temperature to allow the transition into a more gel-like state. Afterward, as represented in Figure 2 b), the material reached a vitreous state by being heated at 80 °C for 3 days, during which the ethanol completely evaporated. Figure 2 c) shows the MBGs after calcination at 700°C for 5 hours, which removes the surfactant and forms the glass structure. Finally, Figure 2 d) displays the MBGs in their final powder form after grinding for 6 hours.

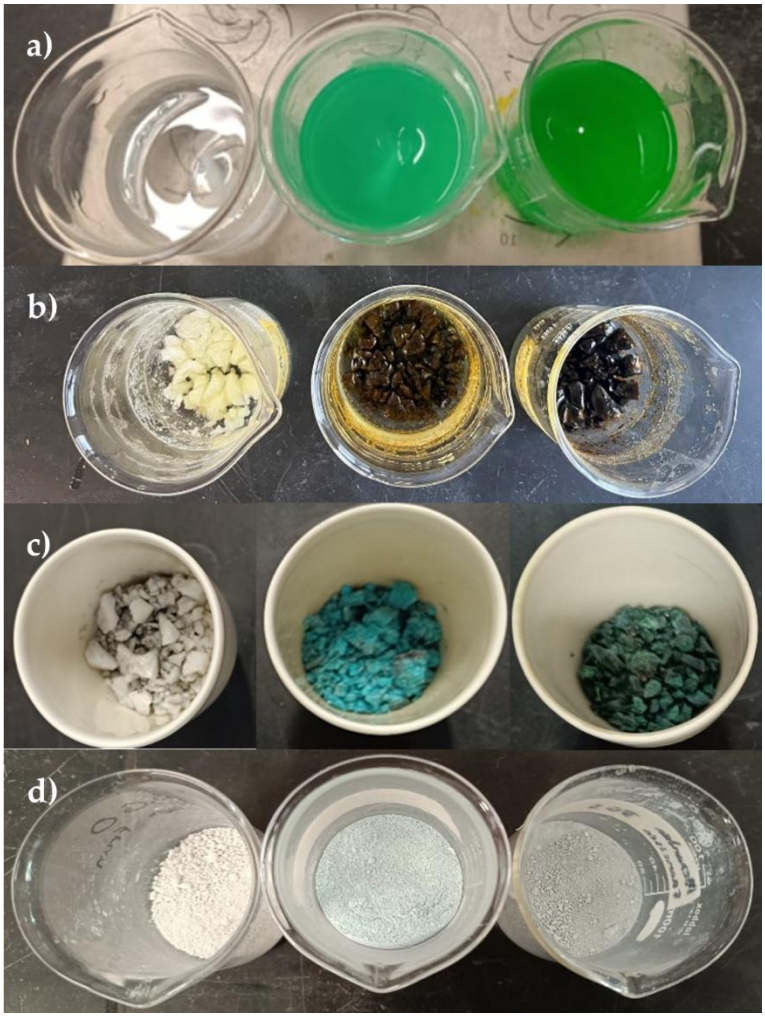

Figure 2 - Representative photographs of bioglasses in different states of production. Each figure follows the same order, with bioglass with 0 mol.% copper (BG0) represented in the left, bioglass with 2 mol.% copper (BG2) in the center, and bioglass with 5 mol.% copper (BG5) in the right; a) sol-gel; b) vitreous; c) glass; d) powder form.

FTIR spectra were analyzed, as shown in Figure 3, revealing three characteristic bands presented across all MBGs, typical of silicate glasses [23]. These bands, located at 1045, 796, and 443 cm^{-1}, correspond to the asymmetric stretching, symmetric stretching, and bending vibrations of Si-O-Si, respectively [13], [24]. Additionally, a band at 935 cm^{-1} was observed specifically in BG5, which is attributed to the vibration of non-bridging oxygen in Si-O-NBO [13], [24]. The presence of this band suggests the introduction of modifiers into the silicate network, which is likely due to the incorporation of copper. This band can be attributed to the Si-O-Cu bonds, indicating that copper has been integrated into the glass structure, affecting the connectivity of the silica network by creating non-bridging oxygens [13].

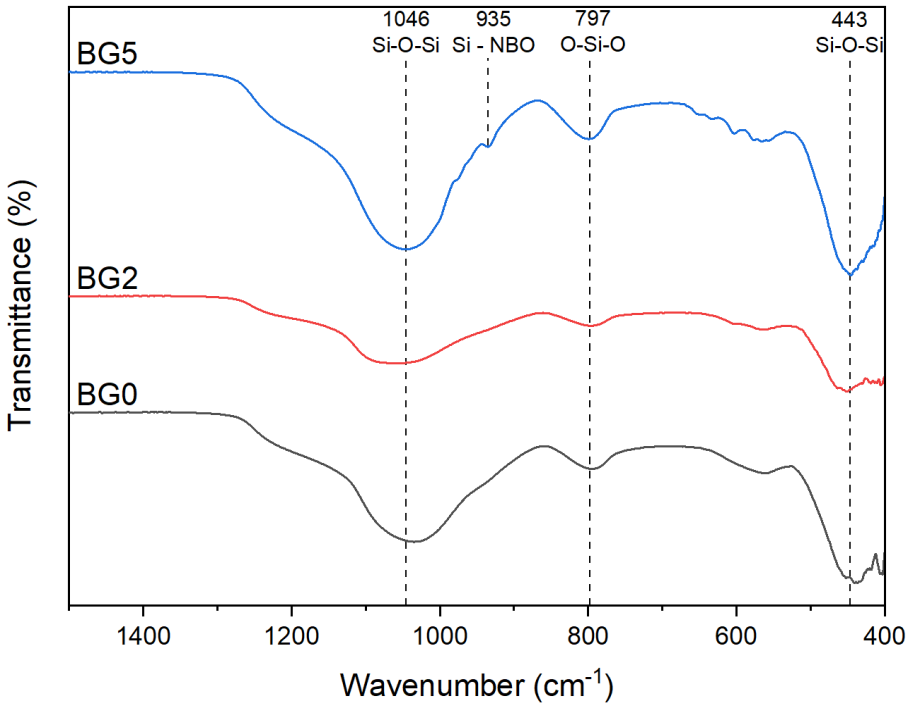

Figure 3 - FTIR spectra of MBGs, where bioglass with 0 mol.% copper (BG0) is represented in black, bioglass with 2 mol.% copper (BG2) in red, and bioglass with 5 mol.% copper (BG5) in blue.

The XRD patterns of all MBGs exhibit a broad hump around 2θ = 20-25°, which is characteristic of amorphous silicate structures. For BG0, this is the only peak present, confirming a completely amorphous silicate structure with no crystalline phases [13]. However, with the introduction of copper, the MBGs displayed partial crystallization. According to JCPDS data (48-1548) for monoclinic CuO (copper oxide), BG2 shows a single crystalline peak at 31.5°, corresponding to the (110) crystal plane, while BG5 reveals three CuO peaks at 31.5° (110), 35.5° ($\bar{1}11$), and 38.8° (111) [25], [26]. These findings, presented in Figure 4, indicate that increasing the copper content enhances the crystallinity of the bioglass [26].

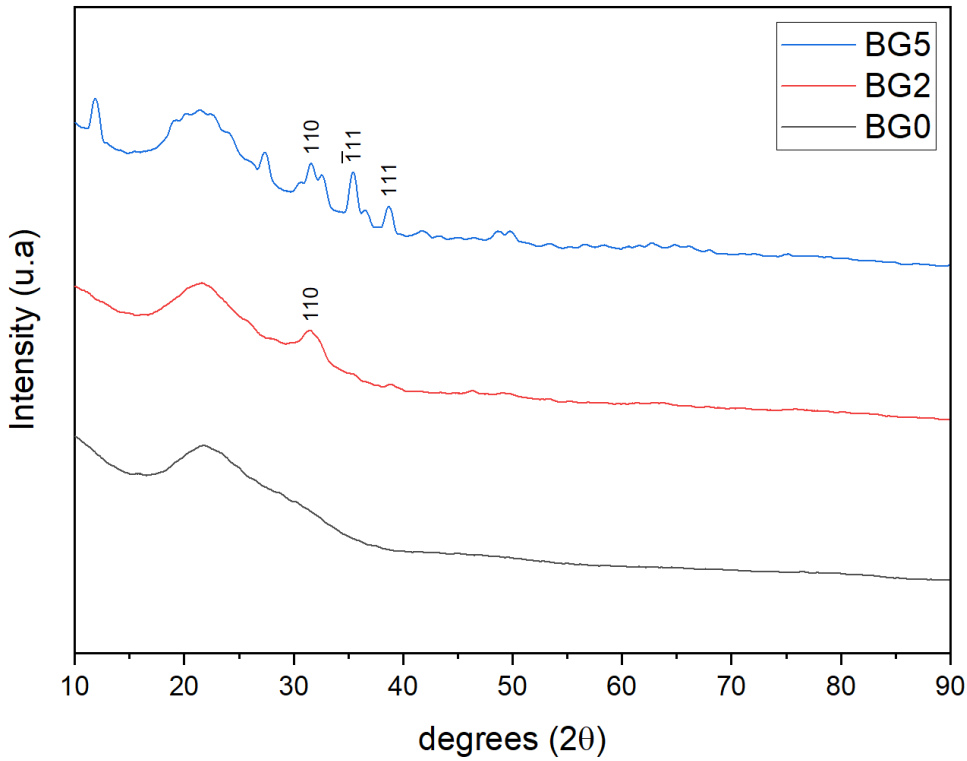

Figure 4 - XRD spectra of MBGs, where bioglass with 0 mol.% copper (BG0) is represented in black, bioglass with 2 mol.% copper (BG2) in red, and bioglass with 5 mol.% copper (BG5) in blue.

LDA was performed to determine the particle size distribution within the different MBGs, where d(0.1), d(0.5), and d(0.9) represent the sizes below which 10 %, 50 %, and 90 % of the particles fall, respectively. In Figure 5 a), BG0 has a relatively narrow particle size distribution with a median particle size of 2.324 µm. The distribution is uniform, with particles mostly ranging between 1.172 µm and 4.179 µm, which indicates a consistent particle size with minimal outliers.

BG2 shows a shift toward smaller particle sizes compared to BG0, as represented in Figure 5 b). The d(0.1) and d(0.5) values are lower, 0.629 µm and 1.263 µm, respectively, indicating that BG2 has finer particles on average. However, the d(0.9) value suggests some larger particles are still present, with a value of 3.752 µm, though not as large as in BG0. The overall distribution is still relatively uniform, but with smaller average particle sizes.

BG5 presents a significantly wider particle size distribution, with d(0.1), with a value of 1.026 µm, and d(0.5), with a value of 2.612 µm, values comparable to BG0, indicating similar small-to-medium particle sizes, as represented in Figure 5 c). However, the d(0.9) value of 17.934 µm is much higher, suggesting that a significant proportion of particles are much larger, possibly due to agglomeration or irregular synthesis conditions with higher copper content.

This indicates a less uniform distribution, with some very large particles skewing the distribution.

All MBGs achieved mean particle sizes below 3 µm, smaller than those reported by Sepulveda *et al.* [27], where bioglass was synthesized using the sol-gel technique with 60 % SiO_2, instead of the 80 % used in this work. In this paper, the bioglass with the smallest particle size (~5-20 µm) exhibited a significantly higher dissolution rate than those with larger particles. This faster dissolution resulted in a more rapid formation of the apatite layer, with the bioglasses' surface completely covered by highly crystalline hydroxycarbonate apatite within the first hour of immersion in SBF.

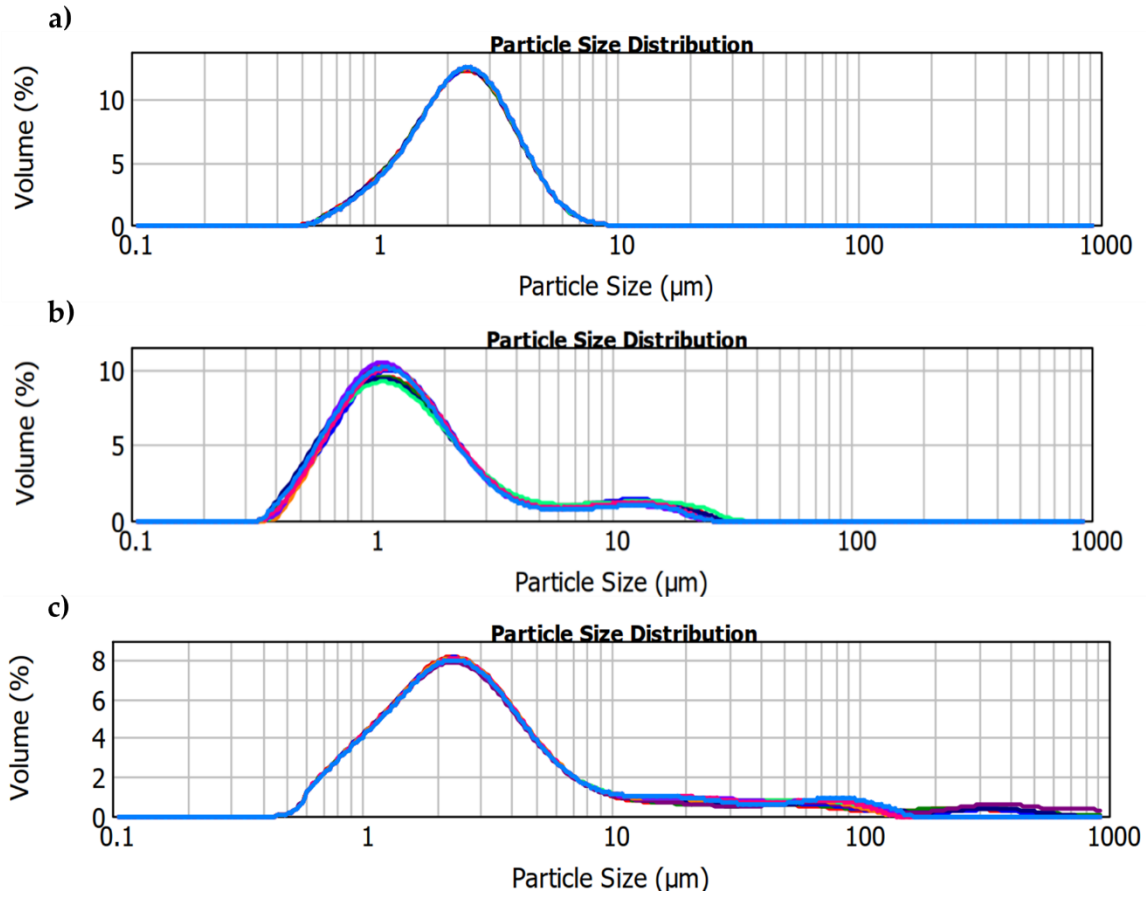

Figure 5 - LDA spectra of MBGs for a) bioglass with 0 mol.% copper (BG0), b) bioglass with 2 mol.% copper (BG2), and c) bioglass with 5 mol.% copper (BG5).

N_2 adsorption-desorption analysis was performed and presented in Figure 6. All MBGs assumed a type IV isotherm pattern, characteristic of mesoporous silica-based bioactive glasses, according to the literature [18], [28]. BG2, even though it does not have a sharp knee, still shows a difference between the adsorption and desorption slopes, therefore not being

considered a type II isotherm pattern, where this difference could be due to larger pores or less uniformity in pore size distribution [29].

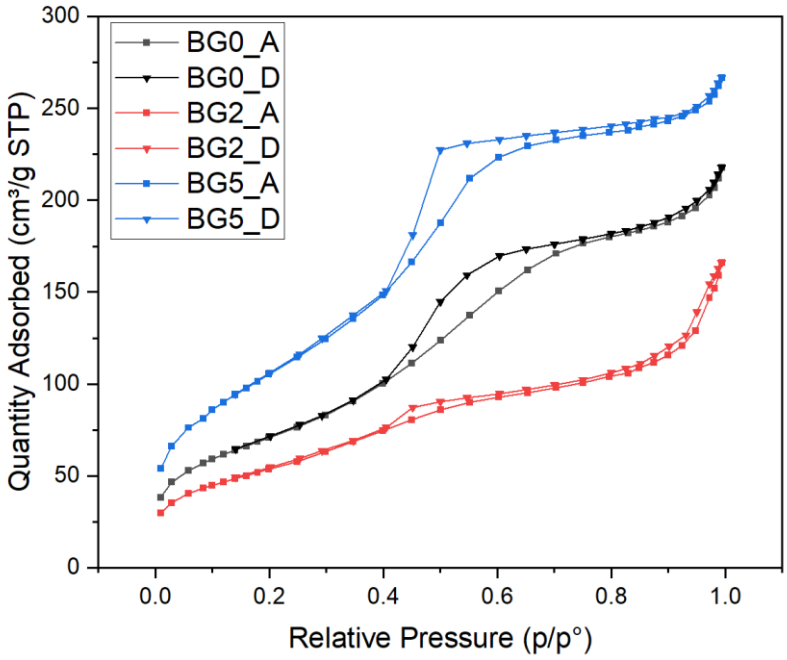

Figure 6 - BET analysis of MBGs, where bioglass with 0 mol.% copper (BG0) is represented in black, bioglass with 2 mol.% copper (BG2) in red and bioglass with 5 mol.% copper (BG5) in blue. Each adsorption line is represented by a square, and the desorption line by a triangle.

In terms of surface area, pore volume, and diameter, as represented in Table 1, BG5 has the highest surface area, followed by BG0, with BG2 having the lowest, which is aligned with the N_2 adsorption-desorption figure shown previously, where BG5 is the MBG with the highest quantity adsorbed, then BG0 and BG2. The pore volume follows a similar pattern to the surface area since BG5 has the highest pore volume, followed by BG0 and BG2. In terms of pore diameter, BG5 has, interestingly, the smallest pore diameter, while BG0 has the largest. This suggests that BG5 has more pores (as indicated by its higher surface area and pore volume), but is smaller in size compared to BG0 and BG2. The results were similar to the literature, which shows that for MBGs synthesized using P-123 as the structure-directing agent, the surface area was within a range of 250 - 499 m^2/g, pore volume of 0.40 - 0.73 cm^3/g, and pore diameter of 3.5 - 6.9 nm [10], [30].

Table 1 - BET analysis of surface area, pore volume, and pore diameter for all MBGs.

Sample	Surface area (m^2/g)	Pore volume (cm^3/g)	Pore diameter (nm)
BG0	246.422	0.314	4.810
BG2	187.073	0.227	4.570
BG5	367.176	0.393	3.970

BG0 - bioglass with 0 mol.% copper (BG0); BG2 - bioglass with 2 mol.% copper (BG2); BG5 - bioglass with 5 mol.% copper (BG5).

Mesopore size distribution is shown in Figure 7, revealing that BG0 has a moderate peak at smaller pores (< 10 nm) with a slight increase around 50 nm. This indicates that BG0 pores tend to be smaller but still have some variety of pore sizes. BG2 displays a small peak at smaller pores and a more pronounced peak at around 50 nm, which is quite vast in width, indicating that this sample has a higher concentration of pores in this size range, being much more heterogeneous. BG5, on the other hand, shows a sharp and significant peak for smaller pores and a low peak at 50 nm, meaning that most of the pores are below 10 nm, revealing a structure more homogeneous. BG5 and BG0 behavior was similar to the one achieved by Baino [31], where the significant difference between these two MBGs was the higher peak of BG5, which assumed a more homogenous pore size distribution. The homogeneity observed in BG5 can be attributed to the higher concentration of Cu^{2+} ions. Bivalent ion dopants, such as Cu^{2+}, disrupt the self-assembly of surfactant molecules, reducing the number of surfactant molecules involved in forming each template. As a result, more but smaller template sites are generated. During calcination, these smaller templates transform into a larger number of smaller pores, which increases the material's specific surface area [32].

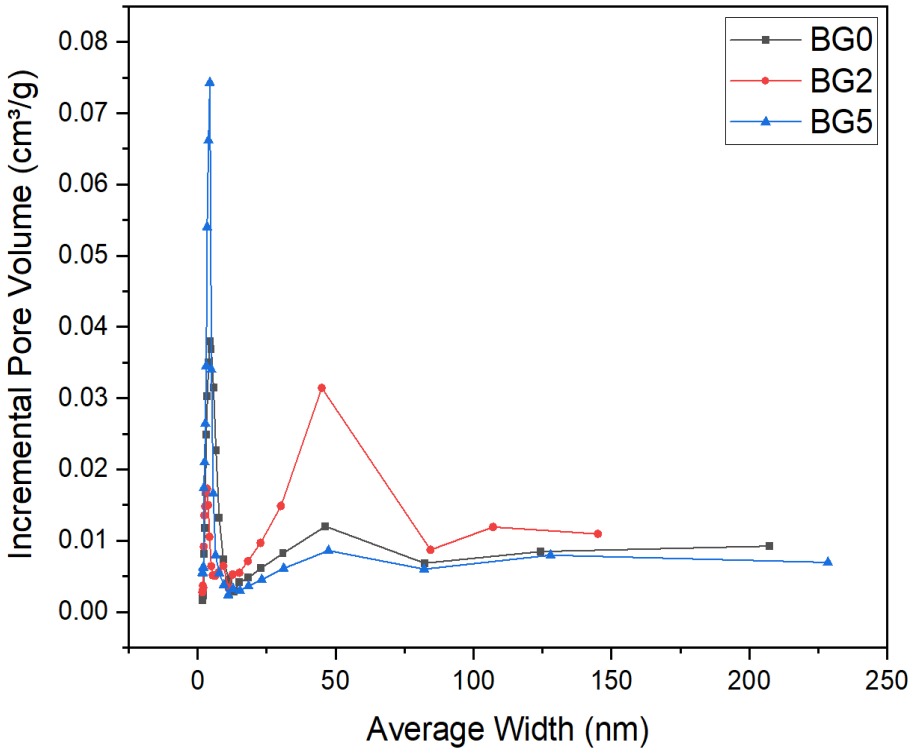

Figure 7 - BET analysis of pore size distribution of bioglass with 0 mol.% copper (BG0), represented in black, bioglass with 2 mol.% copper (BG2), represented in red, and bioglass with 5 mol.% copper (BG5) represented in blue.

STEM analysis shown in Figure 8 was performed on all MBGs, revealing zones with parallel lines, representing the formation of ordered mesoporous channels. The addition of copper did not seem to disrupt the mesoporosity pattern, as the key factors influencing mesoporosity are the surfactant used and the condensation of inorganic precursors through the EISA process [32]. All literature that synthesized bioglasses with P-123 as a surfactant, following the EISA method, reported a parallel arrangement of nano-sized channels, both with and without the incorporation of copper [20], [31], [32]. Upon zooming in on the pores, the structure reveals a hexagonal space-group symmetry, specifically a p6mm structure, aligned along the [001] plane. This is consistent with findings by Yan *et al.* [15], who observed the same p6mm structure in MBGs with a similar mol.% SiO_2 as used in this work.

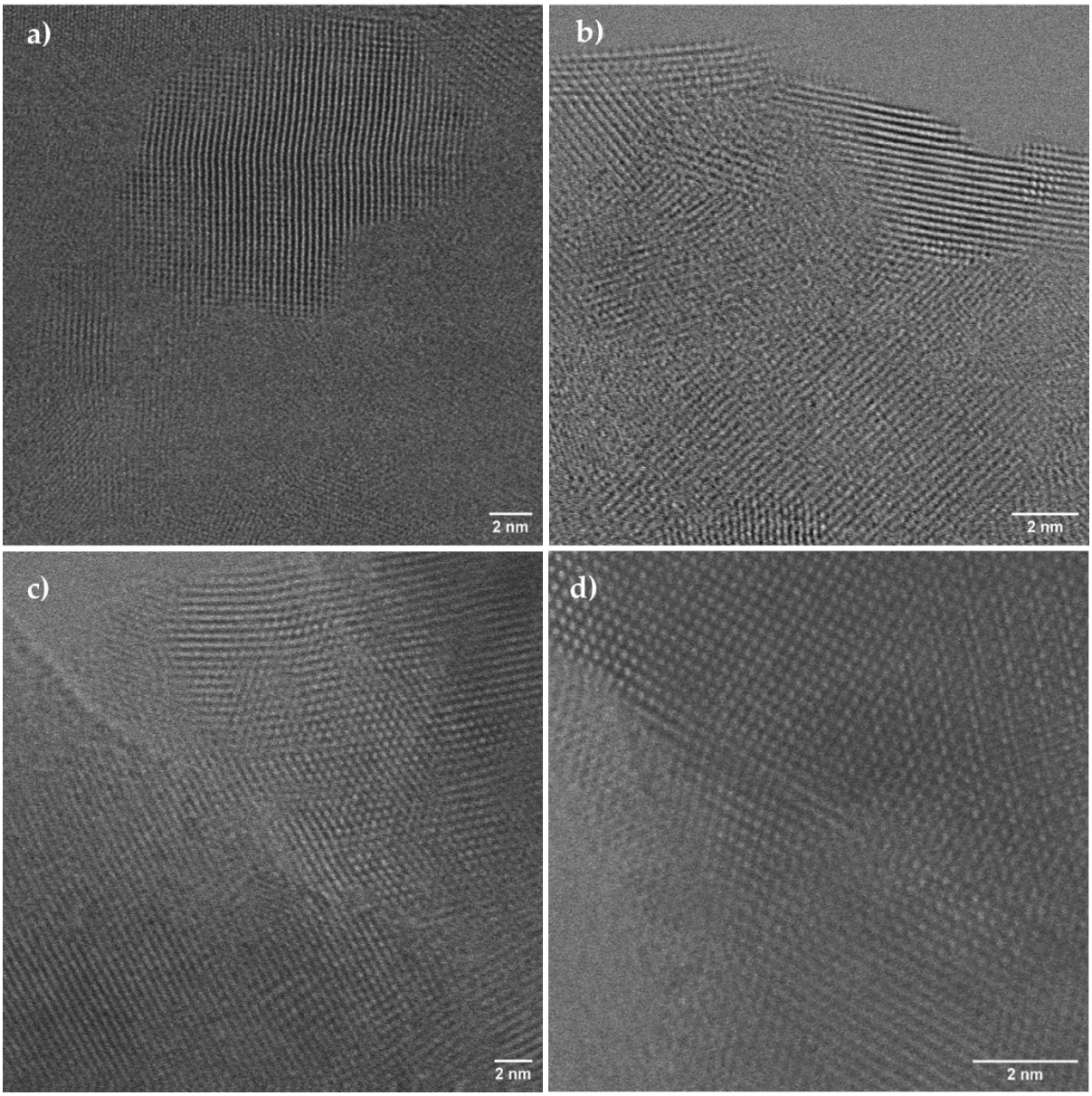

Figure 8 - STEM analysis of a) bioglass with 0 mol.% copper (BG0), b) bioglass with 2 mol.% copper (BG2), and c) bioglass with 5 mol.% copper (BG5). d) A closer look at pores reveals a hexagonal symmetry.

3.2 Bioactivity

A bioactive material is defined as one that induces a specific biological response at its surface, forming a bond between the material and the surrounding tissue [33].

In this case, when bioglass comes in contact with biological fluids, it promotes the formation of a hydroxycarbonate apatite (HCA) layer on its surface, having hydroxyapatite a stoichiometric ratio of Ca/P ~ 1.67 in natural bone [34]. Therefore, the results desired for MBGs bioactivity should be similar to the ratio described to enhance apatite mineralization,

facilitating the integration and bonding with bone tissue [35]. This layer is easily detected by its characteristic spherical structures, similar to cauliflower shapes [36].

To evaluate such an important property, MBG pellets were immersed for different periods of time in SBF, to mimic body fluids at 37 °C, since it is the normal temperature of the body, and the ions release was studied, as well as the pellets surface, to detect any formation of HCA, by SEM.

Figure 9 illustrates the morphology of the pellets 3 hours and 72 hours after the SBF immersion. The rest of the times evaluated by SEM can be observed in figure 17, in section A.2 of the Appendix. It is noticeable for all MBG pellets that after 3 hours, the formation of the apatite layer is already beginning. After 72 hours, the surface of the pellets is fully covered with structures matching the expected morphology. However, the introduction of copper slightly interfered with the bioactivity of the samples, as the size of the apatite spheres appears to decrease with increasing copper concentrations. This reduction could be attributed to the competition between Cu^{+2} and Ca^{+2} ions for the precipitation of phosphate species [37]. Nevertheless, EDS analysis revealed that all MBGs were able to achieve similar Ca/P ratios, although copper-doped MBGs required more time to reach these values. For BG0 a Ca/P ratio of 1.60 was achieved after 72 hours of immersion in SBF, while BG2 achieved a 1.64 ratio after 7 days, as well as BG5, with a value of 1.75. Similar finds were reported by Hammami *et al.* [38], where MBGs with concentrations above 1 mol.% of copper had a decrease of apatite size particles on the surface of the samples, but within 14 days all Ca/P ratios presented a value between 1.70 and 1.79.

These results highlight the potential of MBGs in promoting bone regeneration, as the formation of an apatite layer supports the adsorption of proteins and the adhesion of cells that subsequently proliferate, differentiate, and secrete collagen, aiding in the integration of bioglass with bone tissue [38].

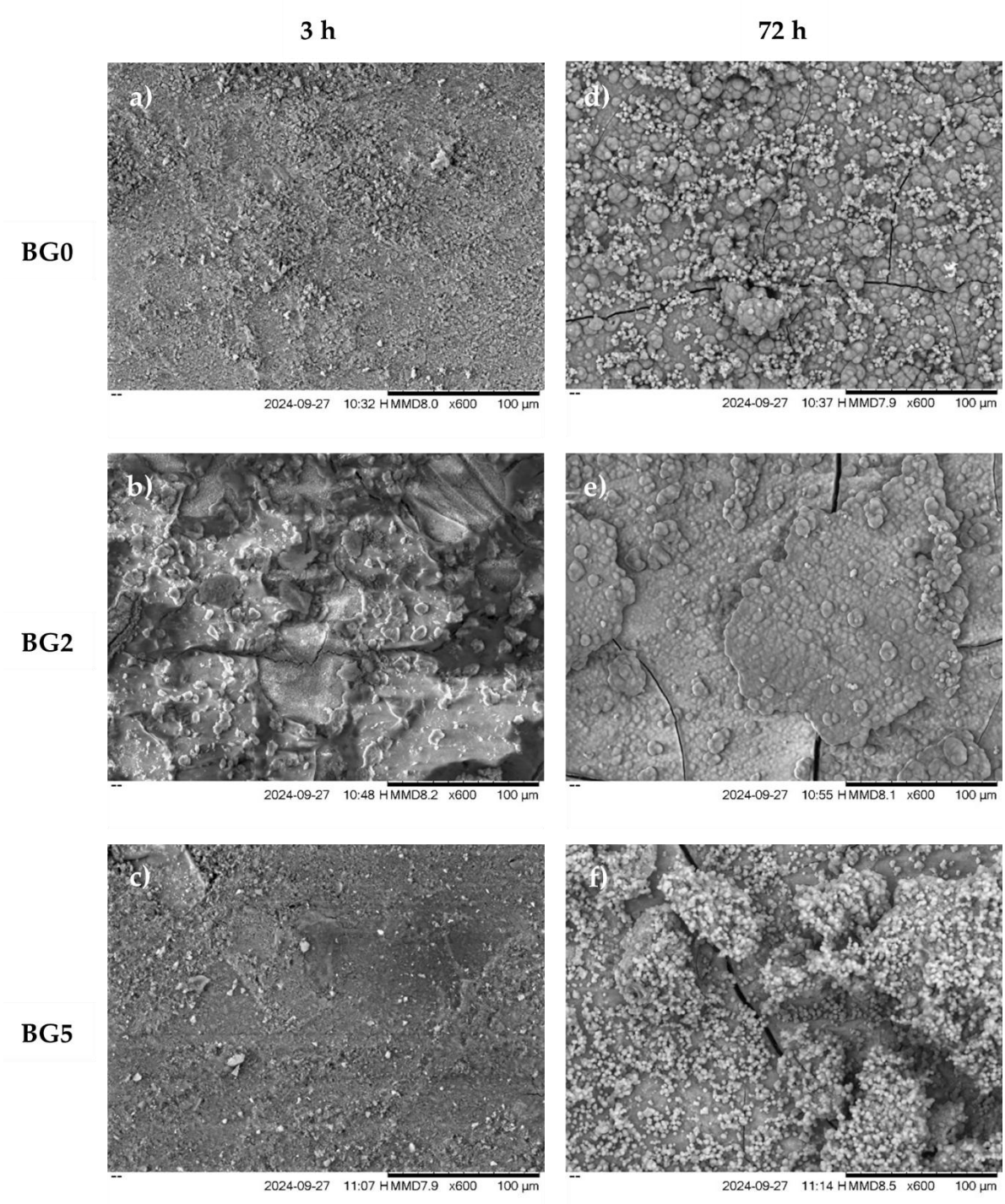

Figure 9 - SEM analysis of MBGs after immersion in SBF for 3 hours (a-c), and 72 hours (d - f). BG0 - bioglass with 0 mol.% copper (a,d); BG2 - bioglass with 2 mol.% copper (b, e); BG5 - bioglass with 5 mol.% copper (c, f).

EDS elemental mapping was also performed, being represented by the EDS of BG5 in Figure 10, with all MBGs achieving a very similar mapping in terms of Ca, P, and Si, which can be observed in figure 18, in section A.2 of the Appendix. All MBGs had an increase of calcium and phosphorus, which can be visualized by the higher contrast of color in Figure 10, after 72

hours of immersion in SBF. Since the surface is filled with the release of these two ions there is a decrease of the silicon content, due to being covered by the new apatite layer [39].

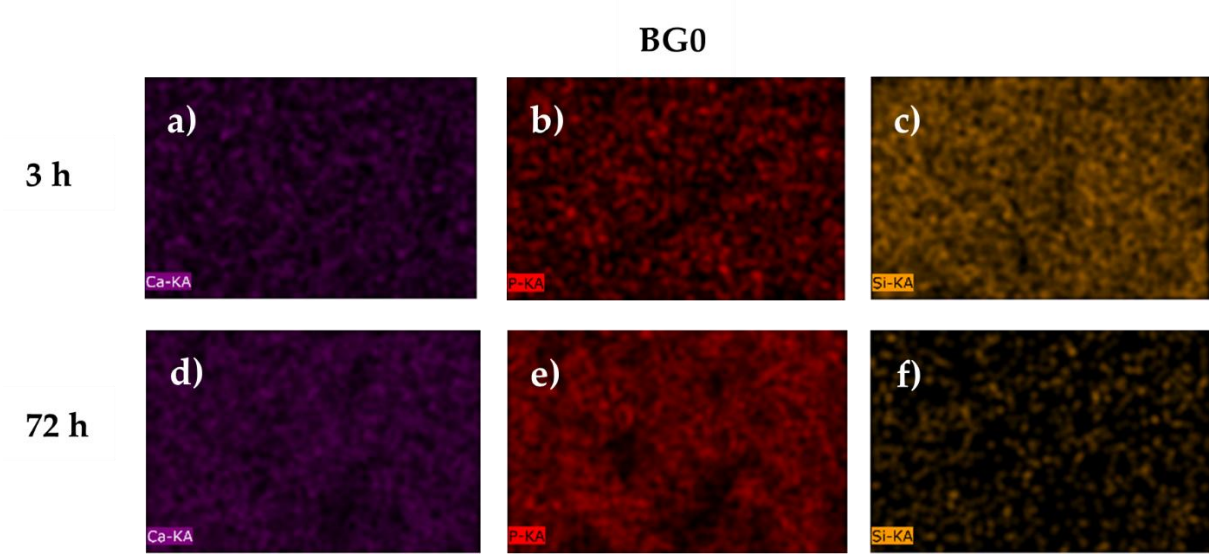

Figure 10 - EDS analysis of bioglass containing 5 mol.% copper (BG5) was performed to represent the elemental behavior in all MBG samples. The distribution of a) calcium (Ca), b) phosphorus (P), and c) silicon (Si) was mapped after 3 hours of immersion in SBF, followed by the analysis of d) calcium, e) phosphorus, and f) silicon after 72 hours of immersion in SBF.

The ICP plots of Ca, P, Si, and Cu ions of all MBGs are presented in Figure 11. In terms of the calcium release to the medium (Figure 11 a)), BG0 shows the highest results, followed by BG2, having both an accentuated peak at 8 hours, and then a decrease until 24 hours, rising again until the value starts to stabilize, and BG5, throughout the 7 days, maintains a constant low release of this ion. For phosphorus (Figure 11 b)), BG0 and BG2 have a decrease until 24 hours, being more stable after that period stamp, and BG5 has a constant release, with BG2 having the lowest result after the 7-day period, being almost null. For the release of silicon ions (Figure 11 c)), all MBGs have similar results throughout the 7 days, with slight fluctuations, achieving all the same concentration in the end. Regarding copper (Figure 11 d)), doped bio-glasses have an identical release, being just BG2 slightly higher than BG5 throughout the period measured.

As stated previously, after the 8-hour mark, both calcium and phosphorus concentrations show an accentuated decrease for BG0 and BG2, due to the formation of the HCA layer that consumes these ions, which supports the SEM and EDS results, and by the end of the 7th day period, both ions appear to have reached their plateau state. These findings were also reported by Ben-Arfa *et al.* [40], where these ions had an initial increasing trend that started to decrease

with the formation of the HCA layer. Also, the soaking time studied in this literature was 28 days, which ultimately confirmed that all ions eventually reached their plateau state.

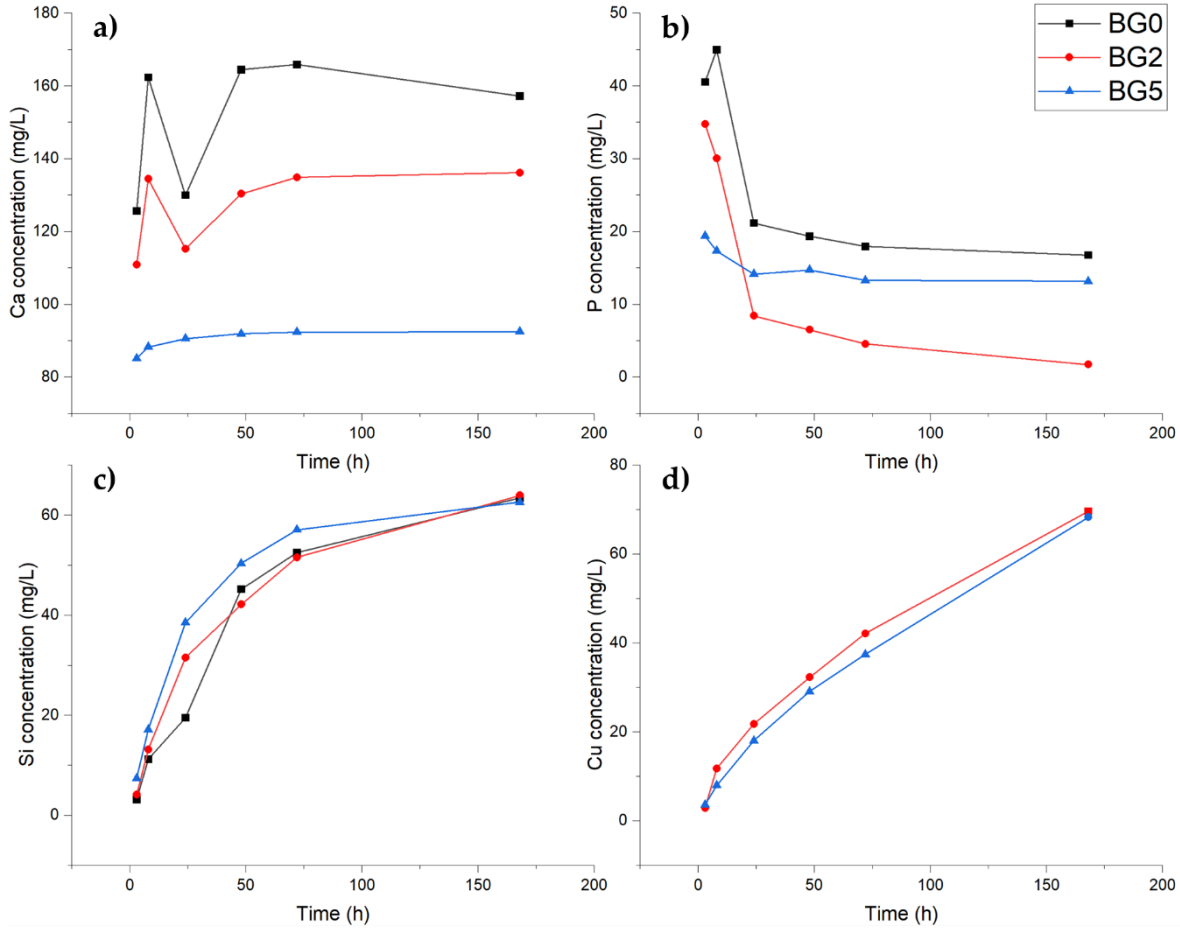

Figure 11 - ICP analysis of ion release in 3 hours, 8 hours, 24 hours, 48 hours, 72 hours, and 7 days in SBF of a) calcium (Ca), b) phosphorus (P), c) silicon (Si), and d) copper (Cu), for bioglass with 0 mol.% copper (BG0) represented in black, bioglass with 2 mol.% copper (BG2), represented in red, and bioglass with 5 mol.% copper (BG5), represented in blue.

3.3 DOX encapsulation efficiency

To evaluate the encapsulation efficiency of DOX, 25 mg of MBGs were immersed in a DOX-PBS solution, with all other parameters held constant. Figure 12 illustrates the encapsulation efficiency across the different MBG variants (BG0, BG2, and BG5) as a function of the initial DOX concentrations in the solution (0.1, 0.2, and 0.4 mg/mL). The encapsulation efficiency (EE (%)), was calculated indirectly by measuring the DOX concentration in both supernatants (PBS and ultrapure water) post-centrifugation and subtracting these values from the initial DOX concentration, as shown in the following equation 1:

$$EE(\%) = \frac{\left(DOX_i - DOX_{pbs} - DOX_{water}\right)}{DOX_i} \times 100 \qquad \text{(Eq. 1)}$$

According to Figure 12, it is noticeable that the encapsulation efficiency had great results for all DOX@MBGs, being suitable to adsorb DOX with a minimum of 75 % efficiency. The encapsulation increased with the initial concentration of DOX, since the medium contains more of the cytotoxic drug instead of PBS. The DOX@MBG with the best result was the BG2, with 0.4 mg/mL concentration, which achieved 97.1 % encapsulation efficiency. Similar results were reported by Wu *et al.* [18], with the nanospheres achieving encapsulation efficiencies of 88.8 %, 92.9 %, and 93 % for DOX concentrations of 0.1, 0.2, and 0.4 mg/mL, respectively. Li *et al.* [41] also demonstrated that mesoporous bioglasses, using gentamicin as the cytotoxic drug, exhibited high encapsulation efficiency, ranging from 79 % to 83 %, while non-mesoporous bioglasses showed significantly lower efficiency, with results between 18 % and 19 %.

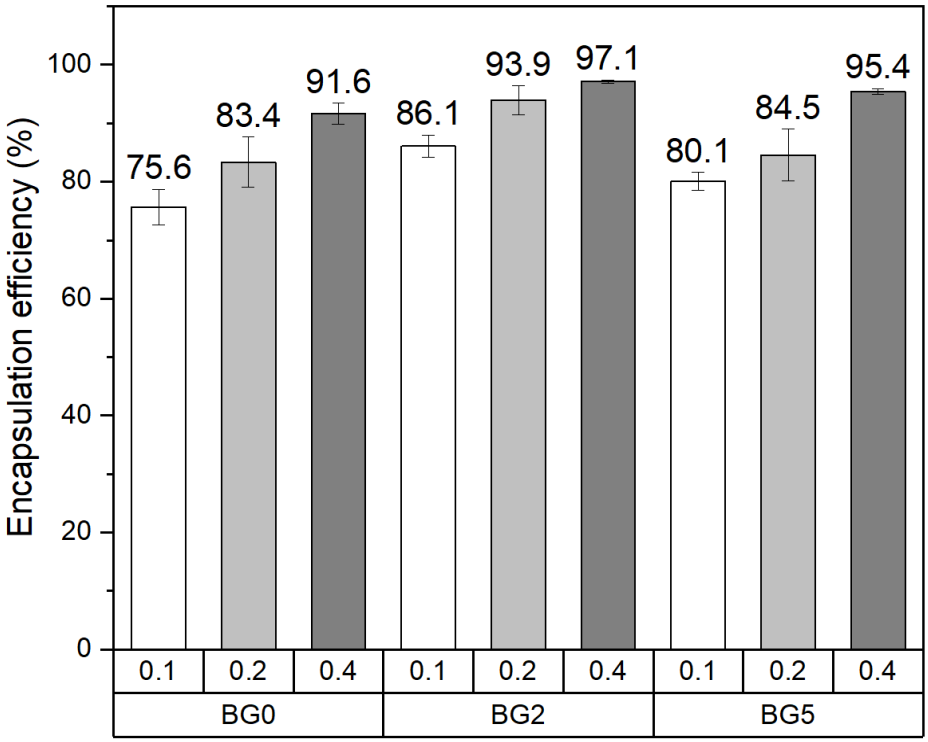

Figure 12 - Encapsulation efficiency of DOX@MBGs with different DOX concentrations (0.1, 0.2, and 0.4 mg/mL), after 7 days of immersion in PBS. BG0 - bioglass with 0 mol.% copper; BG2 - bioglass with 2 mol.% copper; BG5 - bioglass with 5 mol.% copper.

3.4 DOX release

To evaluate the release of DOX, the same 25 mg of DOX@MBGs were immersed in 5 mL of PBS 7.4 pH at 37 °C, and 2 mL were taken out at different times for UV-VIS analysis and replaced with fresh PBS.

The cumulative release was determined by adding the mass of DOX present in each of the 2 mL of PBS taken for analysis at different timestamps and dividing it by the DOX mass that was loaded into the MBG (encapsulated).

As shown in Figure 13 a), b), and c), the release only started after 24 hours, except for BG0, which started before. In general, the cumulative release was proportional to the amount of DOX and inversely proportional to the copper concentration within the samples. Consequently, BG0 exhibited the highest cumulative release, reaching 18.3 % with 0.4 mg/mL of DOX, while BG5 showed the lowest cumulative release, achieving just 1.7 % with 0.2 mg/mL of DOX after 7 days.

It is noticeable that this evaluation had significant deviations, which can be due to the small amount of MBG used for this test, which was only 25 mg for each sample. Regardless, comparing the DOX@MBGs final cumulative release at 7 days, as shown in Figure 13 d), it is noticeable the difference between them, where the cumulative release is inversely proportional to the amount of copper present in the samples. Also, for the sample without copper, BG0, the difference between each DOX concentration is much more prominent, whereas for the other samples, the difference tends to be smaller, being almost indifferent to BG5. This particularity of BG5 is important so that with a higher concentration of DOX, it is possible to achieve a slow release of DOX, since it had similar results as using a smaller concentration.

One of the conclusions taken from Wu *et al.* [18], when studying drug release in MBG nanospheres, is that the pH takes an important role in drug release kinetics, where lower pH (4.0) leads to a quicker release of DOX, achieving a drug release around 30 % after 7 days, than higher pH (7.4), with values around 20 %, similar to the values achieved with BG0 for 0.4 mg/mL. This result is particularly important because the local pH of tumors is more acidic than that of normal tissues, making this therapy more effective in targeting tumor cells than healthy bone cells [18].

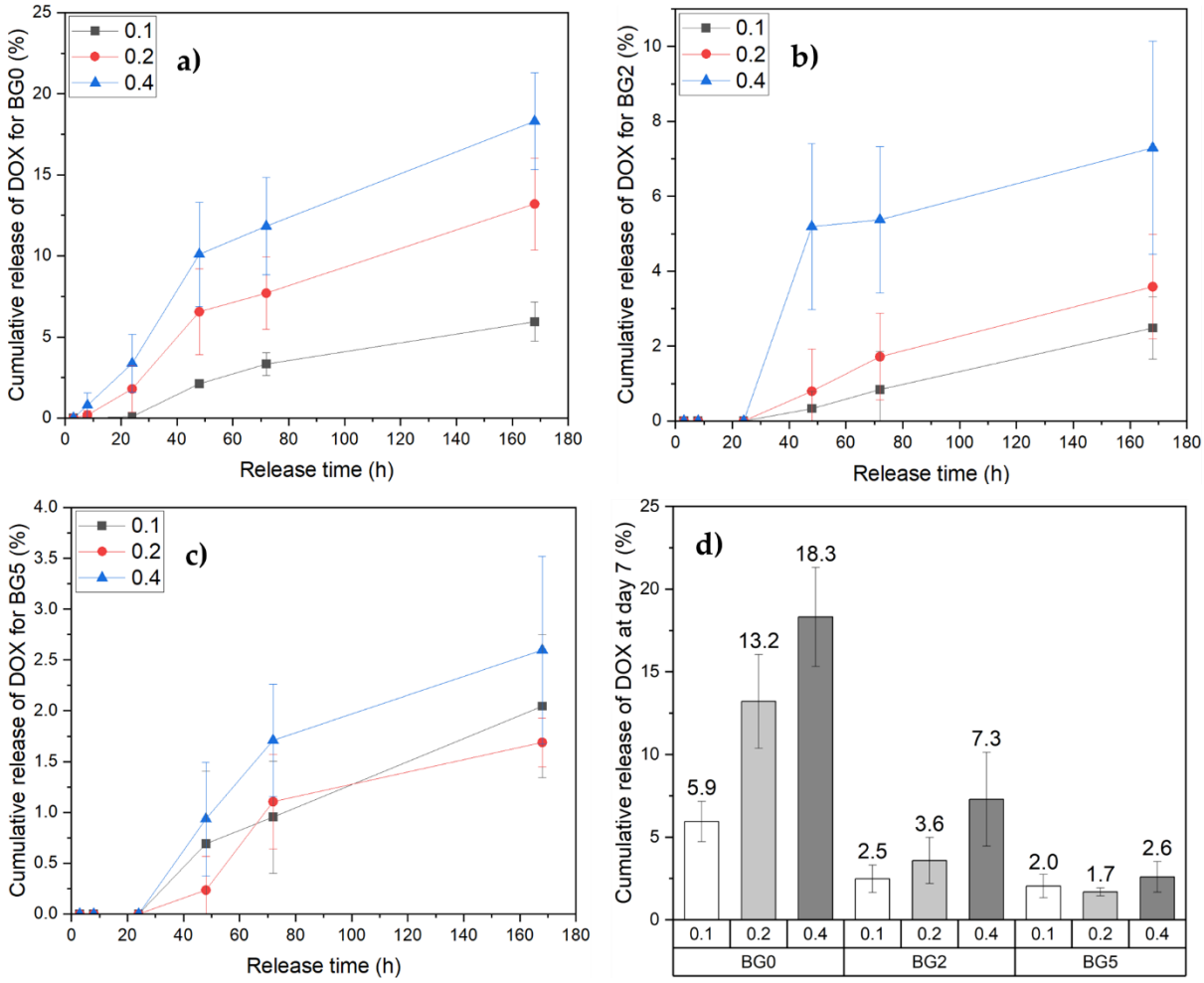

Figure 13 - Cumulative release of DOX for all DOX@MBGs and concentrations of DOX (0.1, 0.2, and 0.4 mg/mL), with timestamps of 3 hours, 8 hours, 24 hours, 48 hours, 72 hours, and 7 days, in PBS. a) bioglass with 0 mol.% copper (BG0), in black, b) bioglass with 2 mol.% copper (BG2), in red, c) bioglass with 5 mol.% copper (BG5), in blue. d) graph bar that represents the cumulative release after 7 days for all MBGs and all concentrations of DOX.

3.5 Anti-bacterial assays

To assess the anti-bacterial effects of MBGs, they were classified as either bacteriostatic (inhibiting bacterial growth and allowing the immune system to gradually eliminate the bacteria) or bactericidal (directly killing bacteria, resulting in their complete elimination) [42].

In Figure 14, each number on the petri dish corresponds to a specific MBG sample that showed no bacterial growth previously. Table 2 and 3 further detail these numbers, correlating them with the respective MBG, its concentration, and its anti-bacterial classification. These results correspond to the first assay performed, but all the replicas achieved the same results, as shown in section A.3 of the Appendix.

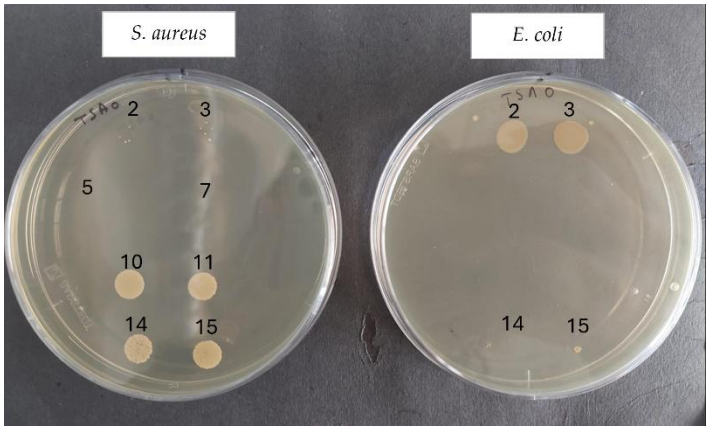

Figure 14 - Bacterial assay 1 for *S. aureus* and *E. coli*. The numbers represent where extracts with no bacterial growth were placed.

As shown in Table 2 and 3, only the copper-doped MBGs exhibited anti-bacterial properties against both bacterial strains, and this effect was observed only at the higher concentrations tested (100 and 50 mg/mL).

These results indicate that BG2 is bacteriostatic for both bacteria at a concentration of 100 mg/mL, while BG5 shows a broader range of effects. Specifically, for *S. aureus*, BG5 at 100 mg/mL is bactericidal, whereas for *E. coli*, the result fluctuated between bactericidal and bacteriostatic, suggesting that this concentration may be the tipping point between the two classifications, where lower concentration means bacteriostatic (as shown for a concentration of 50 mg/mL), and higher concentration would mean bactericidal. In terms of passivated extracts, only BG5_P exhibited anti-bacterial properties and only against *S. aureus*, being bacteriostatic with a 100 mg/mL concentration.

Table 2 - Classification of anti-bacterial MBGs for *S. aureus* for assay 1.

S. aureus			
Position	Sample	Concentration (mg/mL)	Classification
2	BG2	100	Bacteriostatic
3	BG2	100	Bacteriostatic
5	BG5	100	Bactericidal
7	BG5	100	Bactericidal
10	BG5	50	Bacteriostatic
11	BG5	50	Bacteriostatic
14	BG5_P	100	Bacteriostatic
15	BG5_P	100	Bacteriostatic

BG2 - bioglass with 2 mol.% copper; BG5 - bioglass with 5 mol.% copper; BG5_P - bioglass with 5 mol.% copper passivated.

Table 3 - Classification of anti-bacterial MBGs for *E. coli* for assay 1.

E. coli			
Position	Sample	Concentration (mg/mL)	Classification
2	BG2	100	Bacteriostatic
3	BG2	100	Bacteriostatic
14	BG5	100	Bactericidal
15	BG5	100	Bacteriostatic

BG2 - bioglass with 2 mol.% copper; BG5 - bioglass with 5 mol.% copper.

As expected, introducing copper enhanced anti-bacterial activity to the MBGs, as one of its multifunctional properties. One of the reasons for this is that bacterial cell walls carry a negative charge due to lipoproteins, while copper ions are released as Cu^{2+}, leading to an electrostatic attraction that can damage the bacterial cell wall, ultimately causing bacterial death [32].

Similar results were obtained by Miola and Verné [43], where bioglass containing a lower concentration of copper did not generate an inhibition zone but effectively prevented bacterial adhesion, whereas bioglass with a higher copper content produced a notable inhibition halo. Soltani-Dehnavi *et al.* [44], when studying the differences between anti-bacterial activity of bioglass with 45 mol.% SiO2, with and without the addition of 1 mol.% copper, achieved the same results for both bioglasses, against *E. coli*, where bactericidal activity began at 12.5 mg/mL. However, for *S. aureus*, the bioglass without copper required 50 mg/mL to achieve bactericidal effects, while the bioglass with copper needed only 25 mg/mL, demonstrating the enhanced anti-bacterial effect of copper.

3.6 Cytotoxicity assays

To evaluate the cytotoxicity of the MBGs, the cell viability was then calculated, according to equation 2:

$$Cell\ Viability\ (\%) = \frac{Absorbance\ of\ treated\ cells}{Absorbance\ of\ negative\ control\ cells} \times 100 \qquad \text{(Eq. 2)}$$

Once the results were obtained, which are detailed in section A.4 of the Appendix, the extracts were then classified as cytotoxic and non-cytotoxic. According to ISO 10993-5, with

viability rates above 70 %, the material poses no significant risk to the organism, as it can be managed by the body's natural pH regulation mechanisms *in vivo* [24].

Figure 15 represents all MBGs and their passivated form, grouped by concentrations, where C1 represents the initial concentration of the extract (100 mg/mL), and D1, D2, and D3 represent the dilutions 50, 25, and 12.5 mg/mL, respectively. The results reveal that the addition of copper made the MBGs severely cytotoxic, with cell viability dropping below 5 % at the initial concentration when compared to MBG without copper, being non-cytotoxic.

For MBGs without copper, BG0 and BG0_P, all concentrations were revealed to be non-cytotoxic, with values exceeding 100 % cell viability. For BG2, there was a significant difference between C1 and D1, with C1 being severely cytotoxic and D1 being slightly above the 70 % limit, being non-cytotoxic, along with D2 and D3, while for BG2_P, all concentrations were non-cytotoxic. Finally, BG5 was the MBG to have both C1 and D1 as severely cytotoxic, with D2 and D3 as non-cytotoxic, having BG5_P even C1 as cytotoxic, with the dilutions being non-cytotoxic.

These results suggest that copper significantly influences cell viability, though passivated extracts still maintain favorable cell viability at the same concentrations. Hammami *et al.* [24], when studying the cell viability of 45S5 bioglass® doped with copper, achieved similar results since passivating the materials reduces the extracts' cytotoxicity, which is primarily linked to a rise in local pH caused by ion-exchange reactions when the sample first contacts the cell culture medium. This interaction breaks down Si-O-Si bonds in the bioactive glass, releasing soluble silica, which increases both the dissolution rate and pH, affecting cellular metabolism. However, passivation helps to mitigate these pH-related effects.

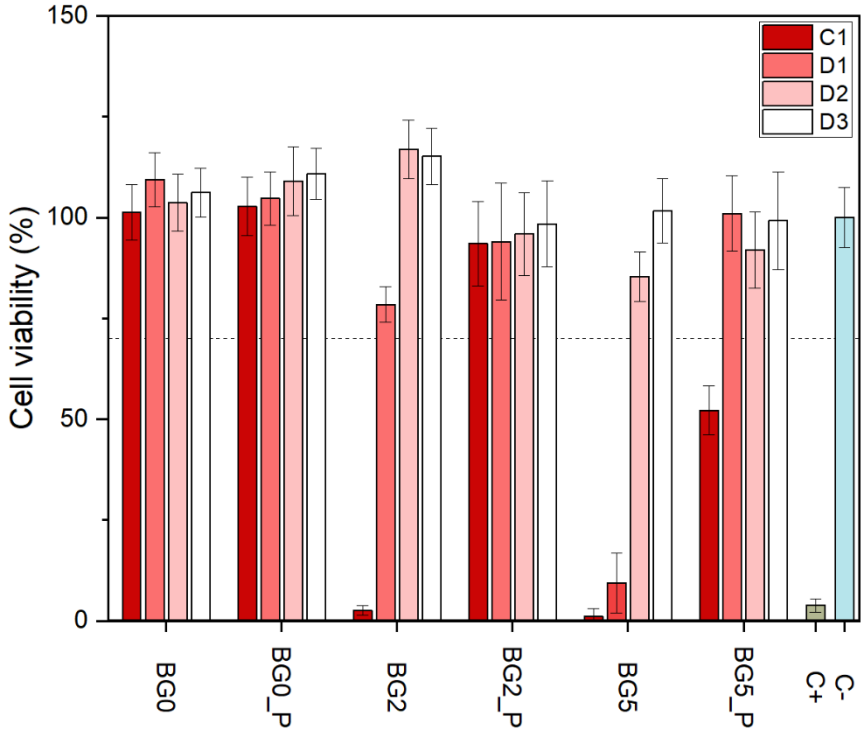

Figure 15 - Cell viability of all MBGs. The horizontal line at 70 % marks the cell viability of no significant risk to the organisms, being considered non-cytotoxic if above it.

4

Conclusion and Future Work

The purpose of this work was to develop mesoporous bioglass-based systems for controlled delivery of cytotoxic drugs, for bone cancer treatment. To achieve this, MBGs were synthesized using the sol-gel method, assisted by the EISA technique, using different molar fractions of copper and calcium to study the differences the introduction of copper would bring to the system since it is known for its additional beneficial properties. Therefore, bioglasses were made with 0, 2 and 5 mol.% of copper. After synthesis, 25 mg of each MBG was loaded with doxorubicin with concentrations of 0.1, 0.2, and 0.4 mg/mL.

Characterization techniques such as FTIR and XRD confirmed the introduction of copper and the amorphous nature of bioglasses. LDA showed all MBGs had a mean particle size below 3 µm, and BET analysis revealed BG5 had the largest surface area (367.176 m^2/g) and pore volume (0.393 cm^3/g) but the smallest pore diameter (3.970 nm). BG2 had the smallest surface area (187.073 m^2/g) and pore volume (0.227 cm^3/g), while BG0 fell in between. Mesopore size distribution revealed that BG5 was the most homogenous in size due to the higher concentration of Cu^{2+} ions, followed by BG0 and then BG2, which was highly heterogeneous. Still, all MBGs revealed a mesoporous particle size since all values were between 2-50 nm. STEM analysis confirmed ordered hexagonal mesoporous channels across all samples due to the zones with parallel lines, where the addition of copper did not seem to disrupt the mesoporous pattern.

Bioactivity studies demonstrated the potential of MBGs to promote bone regeneration, with the formation of an apatite layer within 7 days, achieving Ca/P ratios similar to the ratio present in natural bone. Although the addition of copper slightly reduced the size of the apatite spheres, EDS analysis confirmed that all MBGs achieved similar Ca/P ratios by the end of the study period. BG0 reached a Ca/P ratio of 1.60 after 72 hours in SBF, while BG2 achieved 1.64

and BG5 reached 1.75, both after 7 days. ICP results further supported these findings, showing the consumption of calcium and phosphorus from the SBF medium.

DOX encapsulation studies revealed great results for all MBGs, with a minimum of 75 % efficiency. BG2, with 0.4 mg/mL concentration, was the MBG that achieved the highest value, with 97.1 % of encapsulation efficiency. In terms of DOX release, BG0 exhibited the highest cumulative release, reaching 18.7% with 0.4 mg/mL of DOX, while BG5 demonstrated the lowest cumulative release, at 2.7% with 0.2 mg/mL of DOX, after 7 days in PBS at pH 7.4. This assay demonstrated that the cumulative release was inversely proportional to the amount of copper present in the samples. For the samples with copper, the difference between each DOX concentration tends to be smaller, being almost indifferent to BG5. This particularity is very pertinent, since a smaller concentration of DOX can achieve the same results as a higher concentration.

Anti-bacterial assays demonstrated copper's significant impact on anti-bacterial activity. This was evident since extracts without copper were unable to have anti-bacterial properties for the concentrations studied (100, 50, 25, and 12.5 mg/mL). For *S. aureus*, BG2 was classified as bacteriostatic, for the first concentration of the extracts tested, while BG5 was considered bactericidal for the same concentration and bacteriostatic for the first dilution, with its passivated extract as bacteriostatic for the initial concentration. Regarding *E. coli*, BG2 was once again bacteriostatic for the first concentration, and BG5 assumed a fluctuating between bactericidal and bacteriostatic for the same concentration.

Cytotoxicity assays revealed that copper increased the cytotoxicity of MBGs, reaching severely cytotoxic levels for the highest concentrations studied, while for BG0 all concentrations revealed to be non-cytotoxic, with values surpassing 100 % cell viability. Even though the extracts became more cytotoxic, passivation was able to reduce their toxicity, resulting in non-cytotoxic values for the same concentrations.

Regarding DOX release studies, since all MBGs were able to release the cytotoxic drug, it depends if the system desired needs a slower or higher release of the drug. BG5 proved to be most suitable for slow-release applications, making it a promising candidate for controlled drug delivery in cancer therapies, since all concentrations achieved a cumulative release smaller than 3 % in 7 days, having a prolonged therapeutic effect.

For future work, the drug delivery studies should be performed with more than 25 mg of MBG powder to minimize measurement deviations, and extend the drug release period beyond 7 days, as this study only covered this duration. With more release time, drug release kinetics should also be evaluated to fully understand how the release in MBGs works. Also,

more MBGs with percentages between 2 and 5 mol.% of copper should be synthesized to further explore options for balancing anti-bacterial and cytotoxic effects.

BIBLIOGRAFY

[1] World Health Organization, "Cancer," *WHO*, 2019. [Online]. Available: https://www.who.int/health-topics/cancer#tab=tab_1

[2] F. Bray *et al.*, "Global cancer statistics 2022: GLOBOCAN estimates of incidence and mortality worldwide for 36 cancers in 185 countries.," *CA: A cancer journal for clinicians*, vol. 74, no. 3, pp. 229–263, Apr. 2024, doi: 10.3322/caac.21834.

[3] "Osteosarcoma: Symptoms, What Is It & Treatment," *Cleveland Clinic*, Sep. 2023. [Online]. Available: https://my.clevelandclinic.org/health/-diseases/15041-osteosarcoma

[4] "Key statistics about bone cancer | Bone Cancer Statistics," *American Cancer Society*, 2024. [Online]. https://www.cancer.org/cancer/types/bone-cancer/about/key-statistics.html

[5] "Osteosarcoma," *NHS inform*, Oct. 2024. [Online]. Available: https://www.nhsinform.scot/illnesses-and-conditions/cancer/cancer-types-in-children/osteosarcoma/

[6] J. Jones, "Bioactive glass," *Bioceramics and their Clinical Applications*, pp. 266–283, Jan. 2008, doi: 10.1533/9781845694227.2.266.

[7] D. Bellucci, A. Sola, A. Anesi, R. Salvatori, L. Chiarini, and V. Cannillo, "Bioactive glass/hydroxyapatite composites: Mechanical properties and biological evaluation," *Materials Science and Engineering: C*, vol. 51, pp. 196–205, Jun. 2015, doi: 10.1016/j.msec.2015.02.041.

[8] S. Kargozar, M. Montazerian, S. Hamzehlou, H.-W. Kim, and F. Baino, "Mesoporous bioactive glasses: Promising platforms for antibacterial strategies," *Acta Biomaterialia*, vol. 81, pp. 1–19, Nov. 2018, doi: 10.1016/j.actbio.2018.09.052.

[9] C. Migneco, E. Fiume, E. Verné, and F. Baino, "A Guided Walk through the World of Mesoporous Bioactive Glasses (MBGs): Fundamentals, Processing, and Applications," *Nanomaterials*, vol. 10, no. 12, p. 2571, Dec. 2020, doi: 10.3390/nano10122571.

[10] I. Izquierdo-Barba and M. Vallet-Regí, "Mesoporous bioactive glasses: Relevance of their porous structure compared to that of classical bioglasses," *Biomedical glasses*, vol. 1, no. 1, pp. 140–150, 2015, doi: 10.1515/bglass-2015-0014.

[11] C. Brinker, Y. Lu, A. Sellinger, and H. Fan, "Evaporation-induced self-assembly: Nanostructures made easy," *Advanced Materials*, vol. 11, no. 7, pp. 579–585, May 1999, doi: 10.1002/(sici)1521-4095(199905)11:7<579::aid-adma579>3.0.co;2-r.

[12] S. Kaya, M. Cresswell, and A. Boccaccini, "Mesoporous silica-based bioactive glasses for antibiotic-free antibacterial applications," *Materials Science and Engineering: C*, vol. 83, pp. 99–107, Feb. 2018, doi: 10.1016/j.msec.2017.11.003.

[13] S. Akhtach, Z. Tabia, K. El Mabrouk, M. Bricha, and R. Belkhou, "A comprehensive study on copper incorporated bio-glass matrix for its potential antimicrobial applications," *Ceramics International*, vol. 47, no. 1, pp. 424–433, Jan. 2021, doi: 10.1016/j.ceramint.2020.08.149.

[14] S. Gupta, S. Majumdar, and S. Krishnamurthy, "Bioactive glass: A multifunctional delivery system," *Journal of Controlled Release*, vol. 335, pp. 481–497, Jul. 2021, doi: 10.1016/j.jconrel.2021.05.043.

[15] K. Johnson-Arbor and R. Dubey, "Doxorubicin," *Nih.gov*, May 30, 2019. [Online]. Available: https://www.ncbi.nlm.nih.gov/books/nbk459232/

[16] X. Yan, C. Yu, X. Zhou, J. Tang, and D. Zhao, "Highly ordered mesoporous bioactive glasses with superior in vitro bone-forming bioactivities," *Angewandte Chemie*, vol. 43, no. 44, pp. 5980–5984, Nov. 2004, doi: 10.1002/anie.200460598.

[17] V. -C. Niculescu, "Mesoporous Silica Nanoparticles for Bio-Applications," *Frontiers in Materials*, vol. 7, Feb. 2020, doi: 10.3389/fmats.2020.00036.

[18] C. Wu, W. Fan, and J. Chang, "Functional mesoporous bioactive glass nanospheres: Synthesis, high loading efficiency, controllable delivery of doxorubicin and inhibitory effect on bone cancer cells," *Journal of Materials Chemistry B*, vol. 1, no. 21, pp. 2710–2718, Jun. 2013, doi: 10.1039/c3tb20275e.

[19] M. ur Rahman *et al.*, "Osteogenic silver oxide doped mesoporous bioactive glass for controlled release of doxorubicin against bone cancer cell line (MG-63): In vitro and in vivo cytotoxicity evaluation," *Ceramics International*, vol. 46, no. 8, pp. 10765–10770, Jan. 2020, doi: 10.1016/j.ceramint.2020.01.086.

[20] C. Wu *et al.*, "Copper-containing mesoporous bioactive glass scaffolds with multifunctional properties of angiogenesis capacity, osteostimulation and antibacterial activity," *Biomaterials*, vol. 34, no. 2, pp. 422–433, Jan. 2013, doi: 10.1016/j.biomaterials.2012.09.066.

[21] P. Soares, "Chitosan-based magnetic nanoparticles for osteosarcoma theranostic," *Handle.net*, Dec. 2015, uri: http://hdl.handle.net/10362/1654.

[22] T. Kokubo and H. Takadama, "How useful is SBF in predicting in vivo bone bioactivity?," *Biomaterials*, vol. 27, no. 15, pp. 2907–2915, May 2006, doi: 10.1016/j.biomaterials.2006.01.017.

[23] J. Serra *et al.*, "FTIR and XPS studies of bioactive silica based glasses," *Journal of Non-Crystalline Solids*, vol. 332, no. 1–3, pp. 20–27, Dec. 2003, doi: 10.1016/j.jnoncrysol.2003.09.013.

[24] I. Hammami *et al.*, "Antibacterial Biomaterial Based on Bioglass Modified with Copper for Implants Coating," *Journal of Functional Biomaterials*, vol. 14, no. 7, pp. 369-369, Jul. 2023, doi: 10.3390/jfb14070369.

[25] L. Sayson, J. Lopez, E. Estacio, A. Salvador, and A. Somintac, "Nanostructured CuO thin film deposited on stainless steel using spray pyrolysis as supercapacitor electrode," *Materials Research Express*, vol. 6, no. 12, Jan. 2020, doi: 10.1088/2053-1591/ab6921.

[26] A. Ethiraj and D. Kang, "Synthesis and characterization of CuO nanowires by a simple wet chemical method," *Nanoscale Research Letters*, vol. 7, no. 1, Jan. 2012, doi: 10.1186/1556-276x-7-70.

[27] P. Sepulveda, J. Jones, and L. Hench, "In vitro dissolution of melt-derived 45S5 and sol-gel derived 58S bioactive glasses," *Journal of Biomedical Materials Research*, vol. 61, no. 2, pp. 301-311, May 2002, doi: 10.1002/jbm.10207.

[28] S. Chitra, P. Bargavi, M. Balasubramaniam, R. Chandran, and S. Balakumar, "Impact of copper on in-vitro biomineralization, drug release efficacy and antimicrobial properties of bioactive glasses," *Materials Science and Engineering: C*, vol. 109, Apr. 2020, doi: 10.1016/j.msec.2019.110598.

[29] F. Sotomayor, K. Cychosz, and M. Thommes, "Characterization of Micro/Mesoporous Materials by Physisorption: Concepts and Case Studies," *Acc. Mater. Surf. Res*, vol. 3, no. 2, pp. 34–50, 2018. [Online]. Available: https://www.hyomen.org/en/wp-content/uploads/papers/vol3_no2/sotomayor/sotomayor_40.pdf

[30] C. Wu and J. Chang, "Mesoporous bioactive glasses: structure characteristics, drug/growth factor delivery and bone regeneration application," *Interface Focus*, vol. 2, no. 3, pp. 292–306, Mar. 2012, doi: 10.1098/rsfs.2011.0121.

[31] F. Baino, "Copper-doped ordered mesoporous bioactive glass: A promising multifunctional platform for bone tissue engineering," *Bioengineering*, vol. 7, no. 2, p. 45, May. 2020, doi: 10.3390/bioengineering7020045.

[32] A. Anand, H. Kaňková, Z. Hájovská, D. Galusek, A. R. Boccaccini, and D. Galusková, "Bioresponse of copper–magnesium co-substituted mesoporous bioactive glass for bone tissue regeneration," *Journal of Materials Chemistry B*, vol. 12, no. 7, pp. 1875–1891, Jan. 2024, doi: 10.1039/d3tb01568h.

[33] V. Krishnan and T. Lakshmi, "Bioglass: A novel biocompatible innovation," *Journal of Advanced Pharmaceutical Technology & Research*, vol. 4, no. 2, p. 78-83, Apr. 2013, doi: 10.4103/2231-4040.111523.

[34] H. Monma and T. Kamiya, "Preparation of hydroxyapatite by the hydrolysis of brushite," *Journal of Materials Science*, vol. 22, no. 12, pp. 4247–4250, Dec. 1987, doi: 10.1007/bf01132015.

[35] U. Pantulap, I. Unalan, K. Zheng, and A. Boccaccini, "Hydroxycarbonate apatite formation, cytotoxicity, and antibacterial properties of rubidium-doped mesoporous bioactive glass nanoparticles," *Journal of Porous Materials*, vol. 31, no. 2, pp. 685–696, Jan. 2024, doi: 10.1007/s10934-023-01546-9.

[36] M. Kheradmandfard, K. Mahdavi, A. Kharazi, S. Kashani-Bozorg, and D. Kim, "In vitro study of a novel multi-substituted hydroxyapatite nanopowder synthesized by an ultrafast, efficient and green microwave-assisted method," *Materials Science and Engineering: C*, vol. 117, Dec. 2020, doi: 10.1016/j.msec.2020.111310.

[37] J. Bejarano, P. Caviedes, and H. Palza, "Sol-gel synthesis and in vitro bioactivity of copper and zinc-doped silicate bioactive glasses and glass-ceramics," *Biomedical Materials*, vol. 10, no. 2, Mar. 2015, doi: 10.1088/1748-6041/10/2/025001.

[38] I. Hammami *et al.*, "Exploring the Impact of Copper Oxide Substitution on Structure, Morphology, Bioactivity, and Electrical Properties of 45S5 Bioglass®," *Biomimetics*, vol. 9, no. 4, p. 213, Apr. 2024, doi: 10.3390/biomimetics9040213.

[39] A. Kusyak *et al.*, "Nanostructured sol-gel bioactive glass 60S: In vitro study of bioactivity and antibacterial properties in combination with vancomycin," *Journal of Non-Crystalline Solids: X*, vol. 20, Dec. 2023, doi: 10.1016/j.nocx.2023.100200.

[40] B. Ben-Arfa, I. Palamá, I. Salvado, J. Ferreira, and R. Pullar, "Cytotoxicity and bioactivity assessments for Cu^{2+} and La^{3+} doped high-silica sol-gel derived bioglasses: The complex interplay between additive ions revealed," *Journal of Biomedical Materials Research Part A*, vol. 107, no. 12, pp. 2680–2693, Aug. 2019, doi: 10.1002/jbm.a.36772.

[41] Y. Li *et al.*, "Mesoporous bioactive glass as a drug delivery system: Fabrication, bactericidal properties and biocompatibility," *Journal of Materials Science: Materials in Medicine*, vol. 24, no. 8, pp. 1951–1961, May. 2013, doi: 10.1007/s10856-013-4960-z.

[42] S. Bernatová *et al.*, "Following the Mechanisms of Bacteriostatic versus Bactericidal Action Using Raman Spectroscopy," *Molecules*, vol. 18, no. 11, p. 13188-13199, Oct. 2013, doi: 10.3390/molecules181113188.

[43] M. Miola and E. Verné, "Bioactive and antibacterial glass powders doped with copper by ion-exchange in aqueous solutions," *Materials*, vol. 9, no. 6, p. 405, May 2016, doi: 10.3390/ma9060405.

[44] S. Soltani-Dehnavi, M. Mehdikhani-Nahrkhalaji, M. Rafienia, and A. Doostmohammadi, "Copper-doped and copper-free bioactive glass nanopowders cytotoxicity and antibacterial activity assessment," *Scientia Iranica*, vol. 24, no. 3, pp. 1706–1716, Jun. 2017, doi: 10.24200/sci.2017.4146.

A

APPENDIX A

A.1 DOX calibration curves

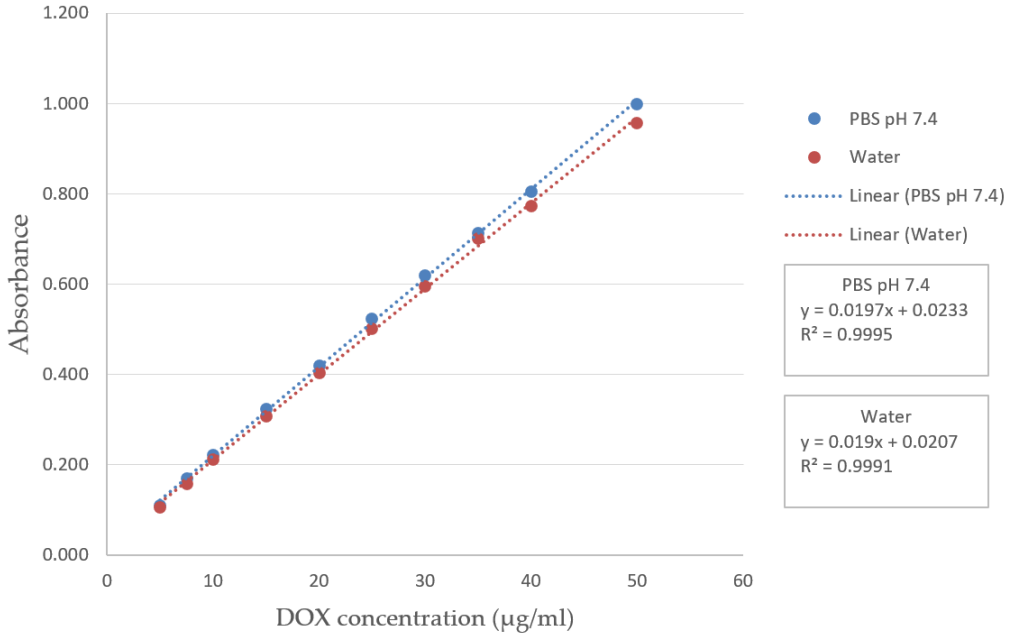

Figure 16 - Calibration curves of DOX in ultrapure water and in PBS pH 7.4 with the respective equations.

A.2 Bioactivity - SEM and EDS analysis of MBGs

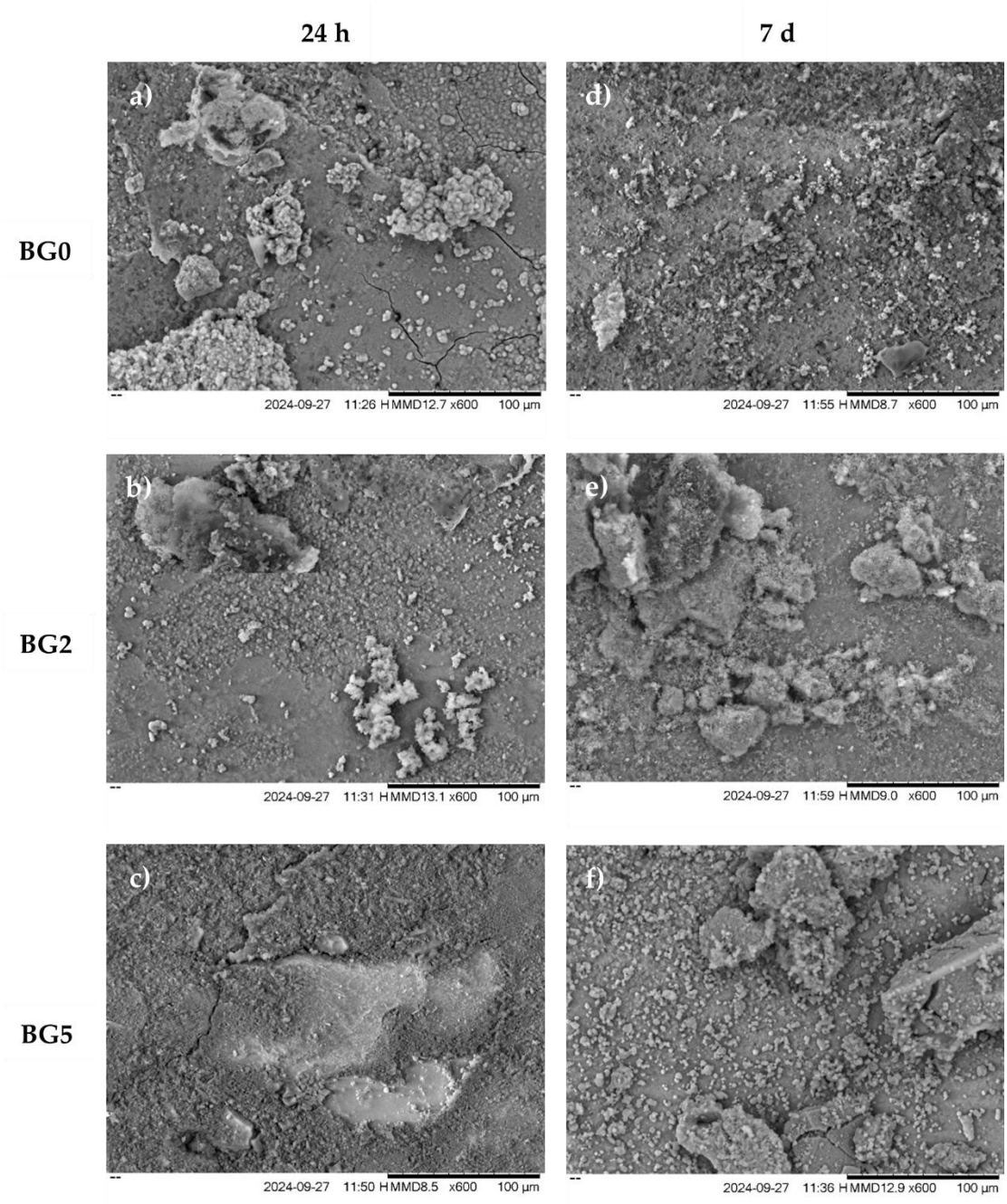

Figure 17 - SEM analysis of MBGs after immersion in SBF for 24 hours (a-c), and 7 days (d - f). BG0 - bioglass with 0 mol.% copper (a,d); BG2 - bioglass with 2 mol.% copper (b, e); BG5 - bioglass with 5 mol.% copper (c, f).

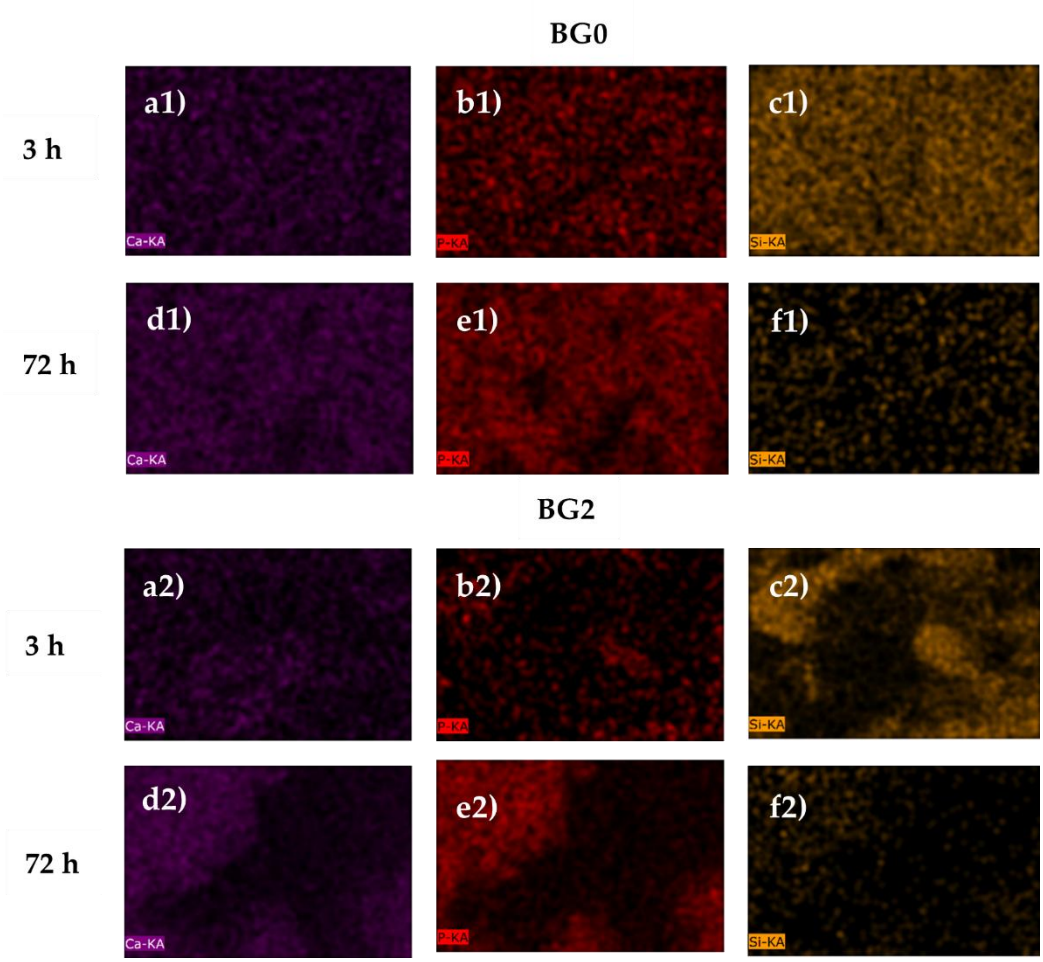

Figure 18 - EDS analysis of bioglass containing 0 mol.% copper (BG0) (a1-f1), and of bioglass containing 2 mol.% copper (BG2) (a2-f2). The distribution of calcium (a1 and a2), phosphorus (b1 and b2), and silicon (c1 and c2) was mapped after 3 hours of immersion in SBF, followed by the analysis of calcium (d1 and d2), phosphorus (e1 and e2), and silicon (f1 and f2) after 72 hours of immersion in SBF.

A.3 Anti-bacterial assays

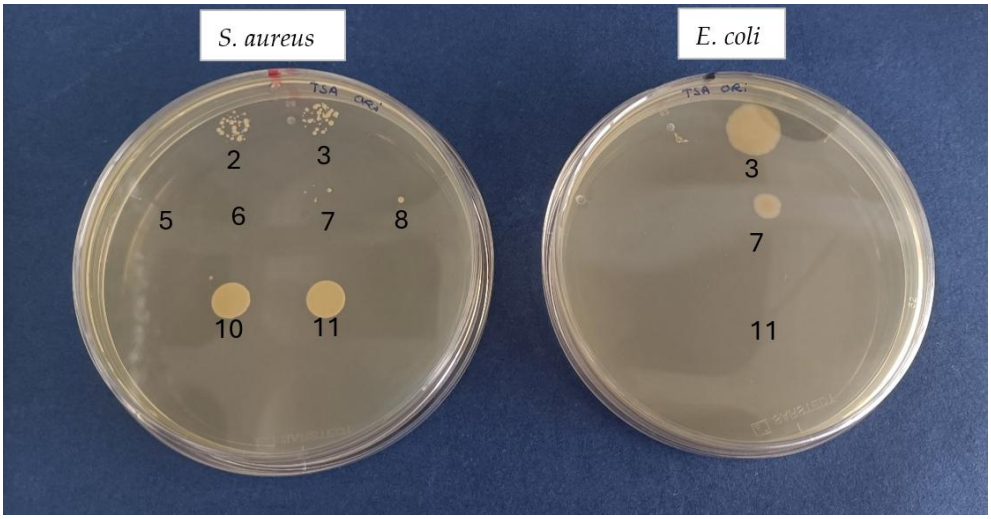

Figure 19 - Bacterial assay 2 for *S. aureus* and *E. coli*. The numbers represent where extracts with no bacterial growth were placed.

Table 4 - Classification of anti-bacterial MBGs for *S. aureus* for assay 2.

Position	Sample	Concentration (mg/mL)	Classification
2	BG2	100	Bacteriostatic
3	BG2	100	Bacteriostatic
5	BG5	100	Bactericidal
6	BG5	100	Bactericidal
7	BG5	50	Bacteriostatic
8	BG5	50	Bacteriostatic
10	BG5_P	100	Bacteriostatic
11	BG5_P	100	Bacteriostatic

BG2 - bioglass with 2 mol.% copper; BG5 - bioglass with 5 mol.% copper; BG5_P - bioglass with 5 mol.% copper passivated.

Table 5 - Classification of anti-bacterial MBGs for *E. coli* for assay 2.

Position	Sample	Concentration (mg/mL)	Classification
3	BG2	100	Bacteriostatic
7	BG2	100	Bacteriostatic
11	BG5	100	Bactericidal

BG2 - bioglass with 2 mol.% copper; BG5 - bioglass with 5 mol.% copper.

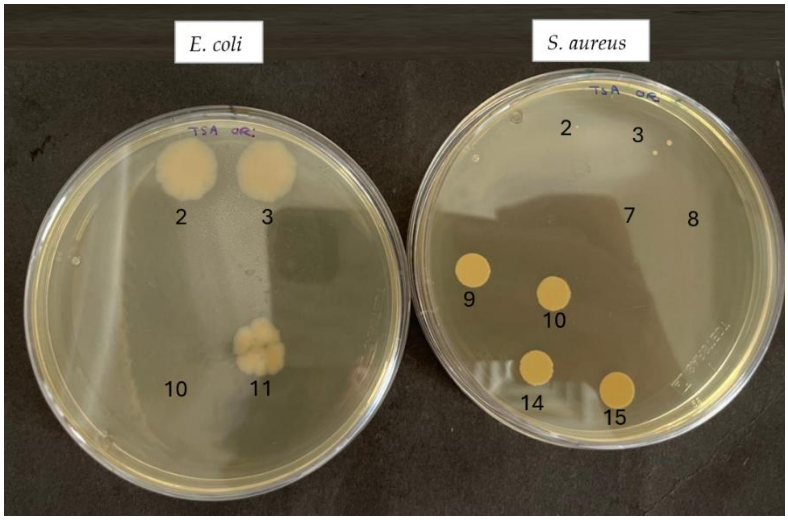

Figure 20 - Bacterial assay 3 for *S. aureus* and *E. coli*. The numbers represent where extracts with no bacterial growth were placed.

Table 6 - Classification of anti-bacterial MBGs for *S. aureus* for assay 3.

Position	Sample	Concentration (mg/mL)	Classification
2	BG2	100	Bacteriostatic
3	BG2	100	Bacteriostatic
7	BG5	100	Bactericidal
8	BG5	100	Bactericidal
9	BG5	50	Bacteriostatic
10	BG5	50	Bacteriostatic
14	BG5_P	100	Bacteriostatic
15	BG5_P	100	Bacteriostatic

BG2 - bioglass with 2 mol.% copper; BG5 - bioglass with 5 mol.% copper; BG5_P - bioglass with 5 mol.% copper passivated.

Table 7 - Classification of anti-bacterial MBGs for *E. coli* for assay 3.

Position	Sample	Concentration (mg/mL)	Classification
2	BG2	100	Bacteriostatic
3	BG2	100	Bacteriostatic
10	BG5	100	Bactericidal
11	BG5	100	Bacteriostatic

BG2 - bioglass with 2 mol.% copper; BG5 - bioglass with 5 mol.% copper.

A.4 Cytotoxicity assays

Table 8 - Cell viability calculations for bioglass containing 0 mol.% copper (BG0).

	BG0				C+	C-
Concentration (mg/mL)	100	50	25	12.5		
Absorbance Subtraction (nm) 570 - 600	0.314	0.354	0.341	0.354	-0.052	0.326
	0.354	0.376	0.344	0.376	-0.039	0.363
	0.358	0.389	0.342	0.359	-0.049	0.310
	0.345	0.382	0.382	0.361	-0.038	0.352
Mean	0.343	0.375	0.352	0.363	-0.045	0.338
St. Dev	0.017	0.013	0.017	0.008	0. 006	0.021
resazurin to resorufin	0.403	0.435	0.412	0.422	0.015	0.398
Cell viability (%)	101.258	109.434	103.648	106.226	3.836	100.000
Uncertainty (%)	6.928	6.698	7.020	6.026	1.670	7.491

Table 9 - Cell viability calculations for passivated bioglass containing 0 mol.% copper (BG0_P).

	BG0_P				C+	C-
Concentration (mg/mL)	100	50	25	12.5		
Absorbance Subtraction (nm) 570 - 600	0.324	0.341	0.398	0.379	-0.052	0.326
	0.376	0.360	0.346	0.390	-0.039	0.363
	0.342	0.348	0.352	0.367	-0.049	0.310
	0.354	0.377	0.398	0.387	-0.038	0.352
Mean	0.349	0.357	0.374	0.381	-0.045	0.338
St. Dev	0.019	0.014	0.025	0.009	0. 006	0.021
resazurin to resorufin	0.409	0.416	0.433	0.441	0.015	0.398
Cell viability (%)	102.830	104.717	108.994	110.818	3.836	100.000
Uncertainty (%)	7.257	6.554	8.485	6.314	1.670	7.491

Table 10 - Cell viability calculations for bioglass containing 2 mol.% copper (BG2).

	BG2				C+	C-
Concentration (mg/mL)	100	50	25	12.5		
Absorbance Subtraction (nm) 570 - 600	-0.053	0.258	0.397	0.398	-0.052	0.326
	-0.051	0.248	0.393	0.418	-0.039	0.363
	-0.052	0.257	0.401	0.380	-0.049	0.310
	-0.042	0.245	0.430	0.396	-0.038	0.352
Mean	-0.050	0.252	0.405	0.398	-0.045	0.338
St. Dev	0.004	0.006	0.015	0.013	0. 006	0.021

resazurin to resorufin	0.010	0.312	0.465	0.458	0.015	0.398
Cell viability (%)	2.579	78.428	116.981	115.157	3.836	100.000
Uncertainty (%)	1.276	4.432	7.226	7.009	1.670	7.491

Table 11 - Cell viability calculations for passivated bioglass containing 2 mol.% copper (BG2_P).

	BG2_P				C+	C-
Concentration (mg/mL)	100	50	25	12.5		
Absorbance Subtraction (nm) 570 - 600	0.266	0.312	0.324	0.304	-0.058	0.344
	0.322	0.264	0.285	0.348	-0.016	0.342
	0.287	0.254	0.288	0.292	-0.037	0.261
	0.316	0.369	0.331	0.323	-0.037	0.345
Mean	0.298	0.300	0.307	0.317	-0.037	0.323
St. Dev	0.023	0.046	0.021	0.021	0.015	0.036
Resazurin to resorufin	0.366	0.368	0.376	0.385	0.032	0.392
Cell viability (%)	93.550	94.061	95.913	98.404	8.046	100.000
Uncertainty (%)	10.426	14.554	10.345	10.604	4.008	13.023

Table 12 - Cell viability calculations for bioglass containing 5 mol.% copper (BG5).

	BG5				C+	C-
Concentration (mg/mL)	100	50	25	12.5		
Absorbance Subtraction (nm) 570 - 600	-0.058	-0.042	0.272	0.328	-0.052	0.326
	-0.053	0.028	0.259	0.368	-0.039	0.363
	-0.066	-0.031	0.282	0.367	-0.049	0.310
	-0.045	-0.044	0.305	0.315	-0.038	0.352
Mean	-0.056	-0.022	0.280	0.345	-0.045	0.338
St. Dev	0.008	0.029	0.017	0.023	0. 006	0.021
Resazurin to resorufin	0.004	0.038	0.339	0.404	0.015	0.398
Cell viability (%)	1.069	9.434	85.346	101.698	3.836	100.000
Uncertainty (%)	2.020	7.447	6.226	8.015	1.670	7.491

Table 13 - Cell viability calculations for passivated bioglass containing 5 mol.% copper (BG5_P).

	BG5_P				C+	C-
Concentration (mg/mL)	100	50	25	12.5		
Absorbance Subtraction (nm) 570 - 600	0.153	0.326	0.286	0.304	-0.058	0.344
	0.119	0.328	0.277	0.286	-0.016	0.342
	0.145	0.33	0.318	0.369	-0.037	0.261
	0.126	0.324	0.285	0.321	-0.037	0.345

Mean	0.136	0.327	0.292	0.320	-0.037	0.323
St. Dev	0.014	0.002	0.016	0.031	0.015	0.036
Resazurin to resorufin	0.204	0.396	0.360	0.389	0.032	0.392
Cell viability (%)	52.171	101.022	91.954	99.234	8.046	100.000
Uncertainty (%)	6.048	9.380	9.428	12.118	4.008	13.023

2024 ALEXANDRA CORDAS

DEVELOPMENT OF MESOPOROUS BIOGLASS-BASED SYSTEMS FOR CONTROLLED DELIVERY OF CYTOTOXIC DRUGS

NOVA SCHOOL OF SCIENCE & TECHNOLOGY